



Published in final edited form as:

Nat Metab. 2020 August ; 2(8): 775–792. doi:10.1038/s42255-020-0226-5.

Tumor-Reprogrammed Stromal BCAT1 Fuels Branched Chain Ketoacid Dependency in Stromal-Rich PDAC Tumors

Ziwen Zhu^{1,2,3}, Abhinav Achreja^{1,2,3}, Noah Meurs^{1,2,3}, Olamide Animasahun^{1,3,4}, Sarah Owen^{3,4}, Anjali Mittal^{1,3,4}, Pooja Parikh^{1,2,3}, Ting-Wen Lo^{3,4}, Janusz Franco-Barraza⁵, Jiaqi Shi^{6,7}, Valerie Gunchick¹¹, Mara H. Sherman⁸, Edna Cukierman⁵, Andrew M. Pickering⁹, Anirban Maitra¹⁰, Vaibhav Sahai¹¹, Meredith A. Morgan^{7,12}, Sunitha Nagrath^{3,4,7}, Theodore S. Lawrence^{7,12}, Deepak Nagrath^{1,2,3,4,7,*}

¹Laboratory for Systems Biology of Human Diseases, University of Michigan, Ann Arbor, MI, 48109, USA

²Department of Biomedical Engineering, University of Michigan, Ann Arbor, MI, 48109, USA

³Biointerfaces Institute, University of Michigan, Ann Arbor, MI, 48109, USA

⁴Department of Chemical Engineering, University of Michigan, Ann Arbor, MI, 48109, USA

⁵Department of Cancer Biology, Fox Chase Cancer Center, Philadelphia, PA, 19111, USA

⁶Department of Pathology, University of Michigan, Ann Arbor, MI, 48109, USA

⁷Rogel Cancer Center, University of Michigan, Ann Arbor, MI, 48109, USA

⁸Department of Cell, Developmental & Cancer Biology, Oregon Health & Science University, Portland, OR, 97201, USA

⁹Barshop Institute for Longevity and Aging Studies, University of Texas Health Science Center at San Antonio, San Antonio, TX, 78245, USA

Users may view, print, copy, and download text and data-mine the content in such documents, for the purposes of academic research, subject always to the full Conditions of use: http://www.nature.com/authors/editorial_policies/license.html#terms

*To whom correspondence should be addressed: Deepak Nagrath, PhD, Department of Biomedical Engineering, NCRC Bldg 28, Room 3048W, University of Michigan, Ann Arbor, MI, 48109, dnagrath@umich.edu.

AUTHOR CONTRIBUTIONS

Z.Z., A.A. and D.N. designed the experiments. Z.Z. performed most experiments. A.A. and O.A. developed and performed all of the bioinformatics analysis. S.O. and S.N. collected PDAC patient samples, isolated, characterized and developed CTC lines using microfluidics Labyrinth chip. A.A., O.A., N.M., and A.Mi developed and performed all metabolic and mass spectrometry assays. P.P. and T.W.L. assisted with assays. J.F.B. and E.C. provided CAFs and helped with stromal characterization, J.S. helped with patient tissue and IHC. V.G. and V.S. collected patient blood for CTC analysis, M.H.S. provided CAFs and helped with stromal characterization, A.M.P. helped with proteasomal analysis, A.Ma analyzed the data and helped in clinical correlations, M.A.M. and T.S.L. provided tissue slices and helped in designing various experiments. Z.Z., A.A. and D.N. wrote the manuscript with input from co-authors.

“The authors disclose no potential conflicts of interest.”

Competing Interests Statement

A. Ma. receives royalties from Cosmos Wisdom Biotechnologies for a license related to a biomarker test for pancreatic cancer early detection. V.S. is a consultant at Halozyne, QED, Ipsen, and Incyte. V.S. receives funding from Celgene (Inst), Bristol-Myers Squibb (Inst), Agios (Inst), Incyte (Inst), Clovis Oncology (Inst), Debiopharm Group (Inst), FibroGen (Inst), Halozyne (Inst), MedImmune (Inst), Rafael Pharmaceuticals (Inst), and Ipsen (Inst). M.A.M. receives honoraria from AstraZeneca. S.N. is the named inventor on a patent for Microfluidic Labyrinth Technology granted to the University of Michigan. S.N. is the co-founders of Labyrinth Biotech Inc. The funders and the company had no role in the design of the study; in the collection, analyses, or interpretation of data; in the writing of the manuscript, or in the decision to publish the results.

¹⁰Department of Translational Molecular Pathology and Sheikh Ahmed Center for Pancreatic Cancer Research, University of Texas M.D. Anderson Cancer Center, Houston, TX, 77030, USA

¹¹Department of Internal Medicine, University of Michigan, Ann Arbor, MI, 48109, USA

¹²Department of Radiation Oncology, University of Michigan, Ann Arbor, MI, 48109, USA

SUMMARY

Branched chain amino acids (BCAAs) supply both carbon and nitrogen in pancreatic cancers, and their increased levels have been associated with increased risk of pancreatic ductal adenocarcinomas (PDACs). It remains unclear, however, how stromal cells regulate BCAA metabolism in PDAC cells and how mutualistic determinants control BCAA metabolism in the tumor milieu. Here we show distinct catabolic, oxidative, and protein turnover fluxes between cancer-associated fibroblasts (CAFs) and cancer cells and a marked branched chain ketoacid (BCKA)-reliance in PDAC cells in stroma-rich tumors. We report that cancer-induced stromal reprogramming fuels this BCKA demand. The TGF- β /SMAD5 axis directly targets BCAT1 in CAFs and dictates internalization of the extracellular matrix from the tumor microenvironment to supply amino acid precursors for BCKA secretion by CAFs. The *in vitro* results were corroborated with human patient-derived circulating tumor cells (CTCs) and PDAC tissue slices. Our findings reveal therapeutically actionable targets in pancreatic stromal and cancer cells.

Several studies have revealed the significance of branched chain amino acids (BCAAs) in cancer including serving as requisite precursors for protein synthesis, maintaining metabolite pools in the tricarboxylic acid (TCA) cycle, and sustaining production of nucleotides and lipids¹⁻⁴. However, the role of stromal cells in support of BCAA metabolism in tumors is still poorly understood. In pancreatic ductal adenocarcinoma (PDAC), the stromal cells identified as activated pancreatic stellate cells or cancer associated fibroblasts (CAFs) account for up to 90% of tumor volume⁵. Furthermore, cancer cells are known to transform quiescent stromal cells into reactive stromal cells⁶. As such, the transformation entails rewiring of metabolic pathways. Since most studies in pancreatic cancers have focused on systemic or cancer cell autonomous BCAA metabolism, understanding cancer-stromal ecosystem requires insight into the intersection of cancer-associated transformations in the stroma with reprogramming of their BCAA metabolism. Deciphering the precise role of various cellular components in BCAA metabolism of tumors is complicated by conflicting evidence from past studies and the challenging nature of the intricate tumor microenvironment (TME). BCAA oxidation has been found to be pronounced in the mouse pancreas compared to other organs⁷. Conversely, decreased BCAA-uptake has been reported in murine PDACs⁸. Neither systemic *in vivo* BCAA metabolism nor cancer cells' BCAA metabolism alone is sufficient to dissect the stromal role. The difficulty in understanding BCAA metabolism in the tumor milieu is exacerbated by nutrient-scarcity, exchange reactions, and metabolite sharing between cancer and stromal cells^{9,10}. Both, the fibrotic environment and nutrient scarcity are difficult to mimic in aggressive murine PDAC models.

The metabolic fates of the BCAAs, leucine, valine, and isoleucine, are cell- and tissue-dependent. BCAA transaminases (BCAT1/2), first deaminate BCAAs to branched chain α -ketoacids (BCKAs) (Fig. 1a). While BCAT2 is expressed in most adult tissues, BCAT1 is

restricted to the brain and spine, retina, ovaries, testes, pancreas and placenta as per the Human Proteome Atlas¹¹. Interestingly, in normal brain, prostate, testis and pancreas, stromal cells account for higher gene expression of BCAT1 compared to epithelial cells, whereas normal ovaries show the opposite trend (Extended Data Fig. 1a). The second step in BCAA metabolism involves irreversible BCKA oxidation catalyzed by the mitochondrial BCKA dehydrogenase (BCKDH) complex. Further, oxidation of BCKAs results in succinyl-CoA and acetyl-CoA that act as anaplerotic or ketogenic sources for the TCA cycle.

We revealed differential BCAA metabolism in cancer and stromal compartments of PDAC tumors. Our study identified a strikingly higher BCAA catabolic flux in CAFs but increased BCKA oxidative flux in cancer cells. Further, CAF-secreted BCKAs were used for maintaining protein synthesis, augmenting TCA cycle metabolite pools, and increasing oxidative phosphorylation in cancer cells. To corroborate the mechanistic underpinnings discovered in our human CAF and cancer cell-line model, we employed two patient-derived models: circulating tumor cells (CTCs) and tumor slice cultures. Collectively, we elucidated an undiscovered metabolic-signaling crosstalk between PDAC and stromal cells and demonstrated that targeting BCAA metabolism in PDAC tumors could mitigate PDAC aggression.

RESULTS

BCAA catabolism is upregulated in CAFs

To determine differences in BCAT catabolism between stromal and PDAC cells, we analyzed protein and gene expression of BCAT1 and BCAT2 (Fig. 1b-c). Interestingly, we found that CAFs had significantly higher BCAT1 expression compared to PDAC cell lines. In contrast, BCAT2 expression was increased in PDAC cells relative to CAFs. Additionally, PDAC cells displayed higher expression of the BCKDH complex enzymes BCKDHA, BCKDHB, and DBT than CAFs (Fig. 1d). Differential DBT expression was corroborated by immunoblotting (Fig. 1b). These results suggested differential BCAA deamination and oxidation potential in stromal and cancer cell-lines. To corroborate, we analyzed transcriptomic data from The Cancer Genome Atlas (TCGA). Since TCGA tumor samples contain a heterogeneous cell population, we deconvoluted the expression of stromal and epithelial compartments from the bulk transcriptomic profile of tumor samples. Stromal-dominant samples showed higher expression of BCAT1, whereas epithelial or malignant cell-dominant samples showed higher expression of BCAT2, BCKDHA and BCKDHB (Fig. 1e, Supplementary Fig. 1a). Our results were further validated by analyzing ROBO1 expression, which was shown to be highly expressed only in stroma¹². These observations were corroborated from transcriptomic data from independent studies (Extended Data Fig. 1b-d, Supplementary Fig. 1b-d)¹³⁻¹⁵.

PDAC tumors consist of a highly heterogeneous population of cancer, stromal and immune cells^{16,17}. Bulk RNASeq techniques are unable to dissect the true transcriptomic signature of these distinct compartments within the TME. Therefore, we used the high-resolution single-cell transcriptomic profiling¹⁸ to analyze BCAA metabolism of PDAC patients (Fig. 1f-g, Supplementary Fig. 2a). Consistent with bulk expression data, single-cell expression analysis revealed that cells expressing epithelial or malignant markers also expressed

BCAT2 but not BCAT1, whereas cells with fibroblast markers only expressed BCAT1. Further, analysis on another single-cell dataset from PDAC patients¹⁹ showed a similar transcriptomic profile of BCAA genes (Supplementary Fig. 2b). Interestingly, single-cell data from normal pancreatic tissue identified that BCAT1 expression is a feature of CAFs rather than normal fibroblasts, whereas BCAT2 expression is similar in PDAC cancer cells and normal ductal cells (Fig. 1h, Supplementary Fig. 2b). Further, we found higher BCAT1 and lower BCAT2, BCKDHA and DLD expression in stromal compared to epithelial compartments of laser-microdissected tumors (Fig. 1i, Extended Data Fig. 1e). IHC staining similarly revealed that the stromal component had significantly higher BCAT1 expression compared to its epithelial counterpart (Fig. 1j, Extended Data Fig. 2a). We further compared BCAT1 and α -SMA expression in PDAC patient-matched tumor and adjacent normal regions and found that both BCAT1 and α -SMA were highly expressed in CAFs compared to fibroblasts in normal stroma, thereby suggesting that enhanced BCAT1 expression in tumor stroma is associated with distinct desmoplasia differing from normal tissue (Extended Data Fig. 2b).

Since differential gene and protein expression does not always translate to metabolic phenotype, we measured BCAA catabolic flux using ¹³C-labeled BCAAs in PDAC cells and CAFs (Fig. 1k). We observed CAFs had three-fold higher BCAA catabolic flux compared to PDAC cell-lines. To evaluate how essential BCAAs are for CAFs' and cancer cells' proliferation, we cultured them under BCAA deprived conditions. Expectedly, CAFs were resilient to BCAA-deprivation *vis a vis* proliferation, whereas cancer cells were BCAA-dependent (Fig. 1l, Extended Data Fig. 2c-d). The finding that cancer cells not only have reduced BCAA catabolic flux compared to CAFs but require BCAAs for growth suggests that intermediates downstream of BCAAs like BCKAs play a significant role in maintaining metabolic activity in the nutrient-starved pancreatic milieu. The reliance of healthy pancreatic ductal and PDAC cells on BCAA catabolism has been well-characterized⁷, but PDACs rewire their metabolism to maintain their BCAA demand in the nutrient-deprived TME. This becomes important in stromal-rich tumors where BCAT1-expressing CAFs outcompete PDAC cells for BCAAs, creating a uniquely nutrient-stressed environment of PDACs.

BCAT2 regulates BCKA-mediated *de novo* protein synthesis in PDAC cells

To address whether upregulated BCAA deamination in pancreatic CAFs fuels the BCAA demand of cancer cells, we measured the proliferation rate of GFP-labeled PDAC cell lines in direct coculture with patient-derived CAFs or normal fibroblasts (NOFs). Notably, we observed that CAFs completely rescued the loss of proliferation of cancer cells under BCAA-deprivation while NOFs had no effect (Fig. 2a-b and Extended Data Fig. 3a-c). This suggests that CAFs may either be secreting BCAAs or BCKAs. We measured BCKA secretion by CAFs to be around 200 pmol/ μ g protein which increased under BCAA-deprivation to around 300 pmol/ μ g protein (Fig. 2c). Interestingly, we found that under BCAA-deprivation, BCKAs rescued proliferation at concentrations as low as 5-50 μ M, whereas 100 μ M BCAA were needed to obtain a similar effect (Extended Data Fig. 3d). This suggested that BCKAs were a more effective nutrient at lower concentrations compared to BCAAs. Once the CAF-secreted BCKAs are consumed by cancer cells, they may be used

directly for BCKA oxidation through the BCKDH complex to maintain oxidative TCA cycle metabolism. BCKAs can also act as substrates for *de novo* synthesis of BCAAs through reamination by the reversible enzyme BCAT2 (Fig. 2d). Although not explicitly shown before, these newly synthesized BCAAs could maintain *de novo* protein synthesis in cancer. To confirm the fate of BCKAs, we cultured cancer cells with ^{13}C -labeled BCKAs and estimated their contribution towards the TCA cycle and for *de novo* BCAA and subsequent protein synthesis (Fig. 2d). We observed that BCKAs are indeed oxidized and incorporated into the TCA cycle via acetyl-CoA and succinyl-CoA as evident from the ^{13}C -labeled TCA intermediates citrate, malate, and aspartate (Fig. 2d). Interestingly, BCKAs were also utilized for *de novo* protein synthesis and contributed more than 60% of the intracellular BCAA pools under BCAA-deprived conditions (Fig. 2d). Further, ^{15}N -labeled glutamine and serine were found to commensurately contribute the required nitrogen for BCAA synthesis. The constituent BCAAs in the protein achieved 40% enrichment from ^{13}C -labeled BCKAs and 50% enrichment from ^{15}N -labeled glutamine and serine, definitively proving that BCKA-derived BCAAs contributed significantly to *de novo* protein synthesis (Fig. 2d).

To substantiate the functional role of BCAT2 in BCAA metabolism of PDAC cells we silenced BCAT2 using both short hairpin (sh) RNA and CRISPR in PDAC cells. We found that BCAT2 knockdown significantly reduced their growth rate implying that BCAT2 plays an important role in PDAC cells (Fig. 2e-f). BCAT2 knockdown resulted in a decrease in ^{13}C -enrichment of BCAAs obtained after protein hydrolysis, confirming the BCKA-mediated, anabolic, regulatory role of BCAT2 in PDAC (Fig. 2g). Having delineated that BCKAs can contribute towards *de novo* protein synthesis, we next assessed whether CAFs could promote protein synthesis in cancer cells. Measurement of *de novo* protein synthesis revealed that PDAC cells indeed increased protein synthesis in CAF cocultures (Fig. 2h, Supplementary Fig. 3). Consistent with significant enrichment of labeled BCKA-derived BCAAs in hydrolyzed protein, BCKA supplementation restored the loss of newly synthesized protein levels under BCAA-deprivation (Fig. 2i). To establish the essentiality of BCAT2, we cocultured BCAT2-knockdown PDAC cells with patient-derived CAFs (Fig. 2j, Extended Data Fig. 3e). Intriguingly, BCAT2 knockdown in cancer cells had no effect on CAF-mediated rescue of cancer cell-growth under BCAA-deprivation conditions. We further excluded the possibility that BCAAs are directly catabolized from autophagy-induced protein degradation²⁰ by knocking down autophagy related genes (ATG5/7) in CAFs and coculturing them with PDAC cells under BCAA-deprivation. We found that ATG5/7 knockdown did not suppress CAF-mediated rescue of cancer cell-growth under BCAA-deprivation (Extended Data Fig. 3f). Moreover, autophagy inhibitors did not inhibit the rescue effect of CAFs on cancer cell-growth under BCAA-deprivation (Extended Data Fig. 3g). Taken together, these results provide strong evidence of regulation of BCAA metabolism by BCAT2 in PDAC cells.

BCKDH complex is essential for PDAC cells' growth and bioenergetics

Since BCAT2 knockdown did not result in a loss of cancer cell growth in cocultures with CAFs under BCAA-deprivation, we hypothesized that irreversible BCKA oxidative decarboxylation by the BCKDH complex could facilitate biosynthesis. To regulate BCKDH complex activity, we targeted the E2 component encoded by DBT. DBT knockdown

profoundly reduced proliferation and colony formation (Fig. 3a-b, Extended Data Fig 4a-b). In contrast, BCKDH kinase (BCKDK), known to suppress BCKDH activity²¹, had no effect on their growth rate when inhibited in PDAC cells (Extended Data Fig. 4c). In agreement with the essentiality of BCKDH complex, addition of BCKAs under BCAA-deprivation rescued the loss of proliferation in PDAC cells (Fig. 3c, Extended Data Fig. 4d), but not in CAFs (Fig. 3d). To confirm that BCKA-mediated growth-rescue is conferred via the BCKDH complex and not BCAT2, we cultured shDBT cells under BCAA-deprivation. As expected, BCKA-mediated rescue of cancer cell growth was attenuated (Fig. 3e). We then cocultured DBT-knockdown PDAC cells with CAFs under BCAA-deprivation to substantiate the BCKDH-dependent role of CAF-secreted BCKA in maintaining PDAC cells' growth (Fig. 3f, Extended Data Fig. 4e). Notably, DBT knockdown in PDAC cells abrogated the rescue effect from CAFs, thereby validating the role of the BCKDH complex.

Given that complete oxidation of one molecule of KIV, KMV, or KIC can provide 6, 5, or 10 NADH molecules, respectively, BCKA-driven NADH could provide a substantial measure of BCKA-oxidative capacity in cells. To further validate the effect of BCKA oxidation on mitochondrial activity, we used a fluorescent, genetically encoded NADH sensor to measure mitochondrial NADH/NAD⁺ in MiaPaca-2 cells cultured in the absence or presence of either BCAA or BCKA (Fig. 3g-h, Extended Data Fig. 4f). Interestingly, BCKAs increased the mitochondrial NADH/NAD⁺ ratio and corroborated that BCKA oxidation enhances energy metabolism. BCKAs can either be reaminated into BCAAs via BCAT2 or they can be oxidized through the BCKDH complex. To investigate both possible fates, we measured NADH in shDBT, shBCAT2, and PDAC cells under varying α KG/glutamate ratios. DBT knockdown reduced the NADH/NAD⁺ ratio in PDAC cells confirming the involvement of DBT and BCKA oxidation in maintaining this ratio (Fig. 3i, Supplementary Fig. 4a-b). We further increased the ratio of α KG/glutamate by supplementing α KG to reduce reamination of BCKAs and favor oxidation. The increased α KG/glutamate ratio nudges BCKAs towards oxidation, confirmed with the observation of increased NADH/NAD⁺ ratio and PDAC cell-growth (Fig. 3j-k, Supplementary Fig. 4c-d). Since the effect of modulating NADH should directly affect mitochondrial oxygen consumption rate (OCR), we measured OCR with different substrates and varying α KG/glutamate ratios. Increasing the α KG/glutamate ratio (by supplementing α KG) increased the OCR significantly, whereas the converse was true when decreasing the ratio (by glutamate supplementation) (Fig. 3l). Finally, we used BCAT2-knockdown cells and found that adding BCKAs increased NADH (Fig. 3m, Supplementary Fig. 4e-f), thus, substantiating that the two outcomes of BCKAs, affect NADH homeostasis differently. Cumulatively, these experiments show that both fates of BCKAs are relevant in the context of PDAC cells, and BCKAs contribute to both the proliferation and bioenergetic metabolism of PDAC cells.

To identify the dominant substrates contributing towards cellular oxidative capacity, we measured OCR. Remarkably, BCKA-driven OCR in PDAC cells was significantly higher than that of alternative substrates (Fig. 3n, Extended Data Fig. 4g). To dissect the role of BCAT2 and DBT in the oxidative capacity of PDAC cells, we measured the OCR of DBT- and BCAT2-knockdown PDAC cells and found that their OCR was significantly reduced (Fig. 3o, Extended Data Fig. 4h). To associate substrate specificity with BCAT2 and the BCKDH complex, we measured substrate-specific OCR in BCAT2- and DBT-knockdown

cells. Interestingly, there was no change in BCKA-driven OCR in BCAT2-knockdown cells, however, BCAA-driven OCR was significantly reduced (Fig. 3p, Extended Data Fig. 4i). Strikingly, in DBT-knockdown cells both BCAA- and BCKA-driven OCR are significantly reduced (Fig. 3q, Extended Data Fig. 4j). Further, BCKA-driven OCR is higher than BCAA-driven OCR, thereby suggesting that BCKAs are a better fuel source for PDAC cells (Fig. 3p-q). These results strongly suggest that PDAC cells are heavily dependent on BCKAs under BCAA-deprived conditions and DBT is a potential target for exploiting this dependency.

Stromal-BCAT1 regulates BCKA synthesis in PDAC tumors

The mechanistic underpinnings of stromal BCKA secretion are necessary to elucidate its dynamics and targetable vulnerabilities. As the synthesis of stromal BCKA is dependent on transamination by BCAT1, we first inhibited BCAT1 activity using the BCAT1 inhibitor, Gabapentin, and measured BCKA secretion in CAFs²². Indeed, Gabapentin significantly reduced BCKA production and subsequent secretion by 40-50% as observed by the extracellular BCKA concentrations (Fig. 4a). To conclusively associate BCAT1 with CAF-mediated rescue of cancer cells in BCAA-deprived conditions, we added Gabapentin to cocultures (Fig. 4b, Extended Data Fig. 5a-b). Notably, inhibition of stromal-BCAT1 abrogated the CAFs' ability to rescue PDAC cell-growth, whereas addition of BCKA markedly restored it. Gabapentin concentration was selected after assessing its inhibition efficacy on BCAT1 activity (Extended Data Fig. 5a). Similarly, BCAT1 knockdown in CAFs and consequently reduced BCKA secretion, significantly reduced the growth rate of PDAC cells (Fig. 4c, Extended Data Fig. 5c). Importantly, knockdown of BCAT2 in CAFs had no effect on the growth rate of PDAC cells (Fig. 4c). These results suggest that BCKA synthesis in CAFs is severely impacted upon loss of BCAT1 expression or activity.

Activated CAFs in PDAC are known to secrete a vast array of extracellular matrix (ECM) proteins such as collagen, enzymes, and glycoproteins²³⁻²⁵. Therefore, we surmised that under nutrient-scarce conditions of the pancreatic TME, ECM proteins in the milieu could be a source of amino acids for CAFs. It is well-established that stromal cells including fibroblasts internalize ECM proteins through uPARAP/Endo180 (encoded by the MRC2 gene)^{26,27} and its expression is maximal in fibroblasts. However, there is a gap in knowledge regarding the role of ECM uptake by stromal fibroblasts in cancer. To illustrate that CAFs utilize ECM proteins we added collagen I or collagen IV to coculture. As seen in Fig. 4d, both collagen I and IV enhanced PDAC cell growth rate in coculture under BCAA-deprivation but had no effect in monoculture. Further, Gabapentin attenuated ECM protein-mediated rescue of cancer cell-growth by CAFs. We also found that Gabapentin markedly reduced *de novo* protein synthesis (Fig. 4e), and mitochondrial NADH/NAD⁺ ratio in PDAC cells (Fig. 4f). To characterize internalization, confirm uptake and cleavage of ECM proteins by CAFs, we used fluorogenic DQ collagen. We found that collagen uptake in CAFs under BCAA-deprivation increased significantly compared to the BCAA-replete condition and this increase was pronounced in presence of TGF- β (Fig. 4g, Extended Data Fig. 5d). Furthermore, we quantified significantly higher collagen uptake in CAFs compared to PDAC cells (Extended Data Fig. 5e). In concurrence with our previous results, uPARAP/Endo180 expression was found to be much higher in CAFs compared to cancer cells (Extended Data

Fig. 5f-g). Moreover, inhibiting uPARAP in CAFs significantly impacted the uptake of collagen (Extended Data Fig. 6a). Cumulatively, these results indicated that ECM-internalization was indeed high in CAFs, but undetectable in PDAC cells. Measuring intracellular BCAA levels and ^{13}C -enrichment in CAFs cultured with ^{13}C -BCAAs further confirmed this (Extended Data Fig. 6b). Notably, intracellular BCAA levels increased gradually post-deprivation (Extended Data Fig. 6c). In contrast, ^{13}C -enrichment of BCAAs gradually decreased in the same timeframe (Extended Data Fig. 6c), indicating the introduction of unlabeled-BCAAs in BCAA-deprived CAFs from ECM proteins.

We hypothesized that proteasomal proteolysis plays a major role in degradation of ECM internalized by CAFs in nutrient-deprived conditions. Consistent with this notion, both BCAA-deprivation and TGF- β increased the chymotrypsin-like proteasome activity in CAFs, but not trypsin-like and caspase-like protease activities (Fig. 4h and Extended Data Fig. 6d). We further investigated the role of the proteasome in collagen degradation (Fig. 4i) and found that collagen is localized with proteasomes in CAFs, thereby suggesting that ECM proteins are indeed degraded by proteasomes. We further tested our hypothesis by measuring BCKA-secretion from CAFs and PDAC cell growth rate in coculture under BCAA-deprived conditions. We found that Delanzomib, the chymotrypsin-like proteasome activity inhibitor, and MG-132, a proteasomal inhibitor, attenuated ECM protein-mediated rescue of cancer cell-growth by CAFs (Fig. 4j, Extended Data Fig. 6e). These data confirm that collagen is indeed degraded by proteasomal proteolytic activity in CAFs. To further strengthen our findings, we measured CAF-secreted BCKAs in the presence of Delanzomib and found that Delanzomib impeded their ability to secrete BCKAs by 40% (Fig. 4k).

To establish whether internalized ECM proteins are a carbon source for CAF-secreted BCKAs, we cultured CAFs on decellularized ^{13}C -BCAA-labeled ECM proteins (Fig. 4l). We used scanning electron microscopy to characterize the ECM structure, and observed that the CAF-derived 3-D matrix is free of cellular debris and remained attached to the culture surface (Fig. 4m). Secreted ECM proteins were acid hydrolyzed and their constituent BCAAs were found to be enriched 40-50% by ^{13}C -labeled BCAAs (Fig. 4n and Extended Data Fig. 6f-g). We then cultured CAFs with ^{13}C -BCAA-labeled ECM under BCAA-deprived conditions and analyzed the spent media obtained after 48 hours of culture. BCKAs secreted by the CAFs were found to be enriched with ^{13}C derived from the proteolyzed ECM (Fig. 4o). This indicated that CAFs cultured with labeled ECM, internalized and proteolyzed it to maintain intracellular BCAA pools, and produce and secrete BCKAs. Collectively, these results provide strong evidence that the ECM in the pancreatic milieu could serve as a storage pool of BCAAs for CAFs under nutrient-stressed conditions.

BCAT1 is a direct target of the TGF- β -SMAD5 pathway in CAFs

To unravel the mechanism underlying the regulation of BCAT1 expression in CAFs we postulated that cancer cells reprogram fibroblasts to upregulate their BCAT1 expression to meet the cancer cells' demand for BCKAs under BCAA-deprivation²⁸. We first transformed NOFs and MSCs into CAFs by culturing them in PDAC cell-conditioned medium (CM) and measured expression of genes involved in BCAA metabolism. This revealed that increased PDAC CM-mediated activation of NOFs and primary MSCs progressively increased

expression of BCAT1 and activated CAF markers (Fig. 5a-b, Extended Data Fig. 7a-e). Consistent with previous results, there was no change in BCAT2 expression in MSCs and NOFs cultured in PDAC cell-CM. These results were further corroborated when CAFs were exposed to PDAC CM and generating similar upregulation of BCAT1 and no significant changes in BCAT2 and BCKDHA/B (Fig. 5c, Extended Data Fig. 7f). We next asked if these activated-NOFs could acquire PDAC-supporting characteristics of CAFs. Notably, we found that, like CAFs, activated-NOFs completely rescue PDAC cell-growth in BCAA-deprivation conditions (Fig. 5d). Having established that fibroblast activation specifically upregulates BCAT1 expression in CAFs, we sought to elucidate the congruence between NOF-activation pathways and BCAT1 expression. Many pathways of fibroblast activation converge towards TGF- β -based activation²⁹. We assessed if TGF- β could regulate BCAT1 expression in CAFs and surprisingly found that induction of BCAT1 expression by TGF- β is pronounced in CAFs (Fig. 5e). By contrast, TGF- β could neither influence BCAT2 expression in CAFs nor induce changes in BCAT1 expression in PDAC cells (Extended Data Fig. 7g). Importantly, depletion of TGF- β abrogated upregulation of stromal-BCAT1 (Fig. 5f) and α -SMA expression mediated by cancer cell-secreted TGF- β , whereas there was no change in BCAT2 expression (Extended Data Figs. 7h, 8a). We employed a genetic approach using α v β 5-integrin KO CAFs, which become activated upon pre-activated (as opposed to immature/latent) administration of TGF- β in a non-cell autonomous way³⁰. The BCAT1 expression of α v β 5-integrin KO CAFs failed to be activated by PDAC cell-CM (Extended Data Fig. 8b). Additionally, we found that cancer cells secreted TGF- β at several folds higher concentrations compared to CAFs (Extended Data Fig. 8c), thereby corroborating our claim that cancer-cell secreted TGF- β regulates BCAT1 expression.

Previous studies provide evidence that SMAD proteins are the effectors of TGF- β activation and once activated, they regulate gene expression by translocating to the nucleus. NOF activation significantly upregulated SMAD2, SMAD4 and SMAD5 (Fig. 5g and Extended Data Fig. 8d-f). To establish which SMAD directly regulated BCAT1 expression, we performed quantitative ChIP-PCR to elucidate the targets for the BCAT1 binding regions. Our analysis revealed the enrichment of SMAD5 for BCAT1 promoter binding regions compared to the control regions (Fig. 5h and Extended Data Fig. 8g-h). Furthermore, only SMAD5 binding to the BCAT1 promoter regions was increased upon TGF- β activation, while SMAD4 binding was not affected. To further decipher if TGF- β and SMAD5 activation increased BCAT1 promoter activity, we performed a dual luciferase reporter assay and found that incubation with TGF- β strongly increased BCAT1 promoter activity in CAFs (Fig. 5i). Expectedly, the increase of TGF- β -mediated BCAT1 promoter activity is suppressed on treatments with either TGF- β pathway inhibitor, RepSox, or by silencing SMAD5 expression (Fig. 5i). Further, IHC staining confirmed that the stromal component had increased expression of SMAD5 compared to the epithelial compartment (Fig. 5j). SMAD5 inhibition significantly impacted the BCAT1 expression at mRNA and protein levels (Fig. 5k-l). In contrast SMAD4 silencing did not induce any changes in BCAT1 expression. Together, these results provide strong evidence that cancer cell-secreted TGF- β upregulates stromal-BCAT1 activity through SMAD5 activation in stromal cells (Fig. 5m).

Validation using patient-derived CTC and tissue slice models

We further expanded our findings in an alternate human preclinical model to allay any model-specific cell-intrinsic and -extrinsic abnormalities. To replicate tumor-stroma interactions in humans in the context of PDAC-cell BCAA metabolism, and overcome inconsistencies observed in animal models, we have relied on two different patient-derived models: human CTCs and PDAC tissue slices. CTCs shed by the primary tumor are the seeds of metastasis³¹ and are established as potential biomarkers of disease progression^{32,33}. CTCs freshly obtained from PDAC patient blood using the Labyrinth, a label-free size-based inertial microfluidic CTC isolation device³⁴, allowed us to compare their transcriptional profile with CAFs and cells obtained from a healthy subject (Fig. 6a, Extended Data Fig. 9a). It is evident that gene expression of BCKDHA and DBT are higher in Day 0 CTCs compared to healthy controls and CAFs (Fig. 6b). In contrast, BCAT1 expression is much higher in CAFs compared to CTCs (Fig. 6b). These data indicate the clinical relevance and corroborate our observations in the *in vitro* model. We then used patient-derived expanded CTC lines for downstream experiments³⁵. Similar to PDAC cell lines, CTC lines showed lower BCAT1 and higher DBT expression compared to CAFs (Fig. 6c). Consistent with our findings in PDAC lines, CTC lines also had higher BCAT2 and lower BCAT1 expression at the protein level (Fig. 6d). Further, BCKAs could rescue the impeded proliferation of CTC lines under BCAA-deprivation, thereby demonstrating that, similar to their cancer cell-line counterparts, CTC lines are also BCKA-dependent in stromal-rich conditions (Extended Data Fig. 9b). Interestingly, there is a marked increase in BCKA secretion by CAFs when they are cocultured with CTC lines after 6 and 12h (Fig. 6e, Extended Data Fig. 9c). Conversely, we did not find any secretion of ketoacids from cancer cells alone (Extended Data Fig. 9d). We next assessed if anaplerotic substrates other than BCKAs could rescue the loss of growth rate of PDAC cells- and CTC lines under BCAA-deprivation. This could also reveal the role of BCKAs as opposed to other TCA cycle substrates in the oxidative mitochondrial metabolism. Anaplerotic TCA substrates only partially rescued the reduction in growth rate; however, BCKAs could completely rescue the growth of PDAC cells and CTC lines under BCAA-deprivation (Extended Data Fig. 9e). We further corroborated our hypothesis that stromal-BCAT1 maintains BCAA metabolism in a CTC-organoid model (Fig. 6f, Extended Data Fig. 9f-g). Importantly, targeting stromal-BCAT1 reduced proliferation and *de novo* protein synthesis in cytokeratin-positive cancer cells of CTC-organoids (Fig. 6g, Extended Data Fig. 9h-i). Our results substantiate that CAFs maintain their ability to fuel the high BCKA-demand of CTCs in organoids, a system that recapitulates tumor heterogeneity closely.

Having illustrated that CAF-derived BCKAs support BCKA-dependence in CTC-lines we wanted to validate these findings in a setting that mimics the *in vivo* TME. Since tissue slices in *ex vivo* culture retain most components of the TME, they are believed to better recapitulate stromal-rich tumors than other *in vivo* tumor models^{36,37}. We obtained fresh PDAC patient tissue slices (Fig. 6h), validated their viability for fourteen days in culture (Extended Data Fig. 10a), and examined whether simultaneously targeting stromal-BCAT1 and cancer cell-DBT could result in an enhanced therapeutic effect. Remarkably, knocking down either BCAT1 or DBT significantly reduced PDAC cell viability (Fig. 6i, Supplementary Fig. 5). Both PCNA and Ki67-positive cell populations had significantly

reduced cytokeratin-positive cells when DBT or BCAT1 were knocked down in combination compared to individual knockdowns. Further, a reduction in DBT and BCAT1 expression validated our siRNA-DBT and siRNA-BCAT1 silencing (Extended Data Fig. 10b). Moreover, there were no changes in other BCAA-related genes. We then asked if BCKAs were indeed consumed by PDAC cells in our tissue-slice model. Tissue slices were cultured in media containing ^{13}C -labeled BCKAs, and after 48 hours, the slices were harvested to extract intracellular metabolites and intracellular protein. Intracellular BCKAs were found to be enriched between 10% and 40%. BCAAs obtained by hydrolyzing the intercellular tumor-slice protein had 2-15% ^{13}C -enrichment, supporting the concept that ^{13}C -BCKA-derived BCAAs were utilized for *de novo* protein synthesis (Fig. 6j).

We tested if suppressing stromal-BCAT1 could reduce BCKA-mediated *de novo* protein synthesis in cancer cells within tissue slices using SUnSET IF. To specifically analyze cancer cells, we used areas of colocalization of puromycin with cytokeratin, a cancer cell-specific marker. Notably, cancer cell-specific *de novo* protein synthesis was pronouncedly reduced in slices treated with Gabapentin (Fig. 6k, Supplementary Fig. 6). Overall, our results highlight that stromal-BCAT1 not only supports PDAC cell-BCKA demand but also exposes the synthetic lethal vulnerabilities in stromal-rich PDAC by cotargeting stromal-BCAT1 and the cancer-BCKDH complex (specifically DBT) as a clinically relevant therapy.

DISCUSSION

Recent reports conclude that the stromal cells play a major role in mitigating nutrient deficiency in PDAC cells^{17,20,38-41}. Further, it was recently shown that BCAAs contribute around 20% of the carbon in the TCA cycle of pancreatic cells⁷. In contrast, we investigated how stromal-CAFs regulate BCAA metabolism in PDAC cells and discovered that there exists a mutualistic relationship *vis a vis* BCAA metabolism between CAFs and PDAC cells. We found that BCKAs play a significant role in maintaining metabolic activity in the nutrient-starved pancreatic milieu. Unconventionally, CAF-secreted BCKAs were used as substrates for *de novo* BCAA synthesis by the reversible action of BCAT2, and newly synthesized BCAAs maintained *de novo* protein synthesis in cancer cells under BCAA-deprived conditions. Our results provide evidence for dependency on the BCKDH complex and suggest its synergistic involvement with BCAT2 in regulating BCAA metabolism in PDAC cells. Recent studies investigated BCAT2's role in PDAC development and found BCAT2 is elevated in PDAC models^{42,43}. Our work develops further understanding of BCAA metabolism in the PDAC TME, especially in context of the pancreatic cancer-cell centric observations of previous studies. To our knowledge, this is the first report that uncovers heavy reliance on BCKAs in stromal-rich tumors and reveals DBT as a vulnerable target. Concurrently, we observed that BCKA-driven oxidation is only dependent on BCKDH expression and not on BCAT2 expression. These results are in line with Neinst et al⁷, showing that BCKDK inhibitors do not affect BCKDH-mediated oxidation, alluding to a high basal BCKDH activity in the pancreas.

The population of CAFs we focus on herein is the myofibroblasts⁴⁴. Recently identified CAF subpopulations explain the heterogeneity seen in CAFs⁴⁴⁻⁴⁶. These different CAFs may have unique metabolic profiles and therefore warrant future studies to assess the

metabolic role of distinct CAF populations. Further, why slowly-proliferating BCAT1-expressing CAFs' have high BCAA-consumption needs to be uncovered. BCAT1-mediated regulation of epigenetics via α KG² could play a role in α KG-mediated epigenetic regulation observed in stroma^{47,48}. Moreover, the effect of varying concentrations of Gabapentin on LAT transporters in CAFs must be assessed in the future. Here, we used clinically relevant human PDAC-derived *ex vivo* models to corroborate and highlight the impact of the metabolic-crosstalk discovered *in vitro*. Unfortunately, validating these observations in *in vivo* models becomes extremely challenging. One major divergence of mouse models from human PDAC tumors, is the limitation to studying interaction between human PDAC cancer cells and mouse CAFs. A second major challenge is the technological limitation of assessing compartmentalized metabolism *in vivo*, although improvements in mass-spectrometry imaging may allow spatial resolution of metabolites across tissue compartments. Third, most current mouse models suboptimally capture the complex phenotype of desmoplasia, so developments of models capturing desmoplasia in the tumor parenchyma are needed to support the mechanism described here.

Recently, PDAC cells were shown to use ECM proteins for maintaining amino acids levels⁴⁹. We found that CAFs uptake ECM under nutrient-limiting conditions underscoring that ECM uptake through uPARAP receptor is upregulated in fibroblasts⁵⁰. CAFs were previously shown to secrete ECM and induce a fibrotic environment in tumors. Our observations stress that this process is reversed under nutrient-deprived conditions, whereby internalized-ECM is degraded through chymotrypsin-like proteasomal proteolysis. Further investigations are needed to ascertain whether ECM uptake through uPARAP or micropinocytosis is the dominant mechanism in PDAC tumors. Altogether, we reveal BCAA metabolism vulnerabilities in desmoplastic PDAC that are synthetically lethal when cotargeting stromal-BCAT1 and the cancer BCKDH complex, specifically DBT. This bridges the gap between knowledge of BCAA metabolism in stroma and BCKA-utilization in cancer cells.

Methods

Cell Culture

PDAC Cell lines—All the cell lines used in this study were purchased from ATCC, used below passage 25 and continuously cultured in 100 U/ml penicillin and 100 U/ml streptomycin. The Mia Paca-2, Panc-1 and Patu 8988t cell lines were routinely cultured in Dulbecco's modified Eagle's medium (DMEM) with 10% fetal bovine serum (FBS) (Atlanta Biologicals, S11150). AsPc1 and BxPC3 cell lines were routinely cultured in Roswell Park Memorial Institute (RPMI) 1640 (Invitrogen) with 10% FBS. All cell lines were mycoplasma free based on PCR-based assays run every month in the lab.

For metabolic and metabolomics assays, 10% dialyzed FBS (Sigma-Aldrich, F0392) was used. For the rescue experiments, DMEM medium without BCAAs was used (United States Biological).

Fibroblast Cell Culture—Patient-derived fibroblast cells were kindly provided by Drs. Edna Cukierman, Anirban Maitra and Mara Sherman and internal STR profiling was

maintained and checked annually. CAFs were cultured at 37°C under 5% CO₂ using DMEM supplemented with 10% FBS and 100 u/ml-mg/ml penicillin-streptomycin. Normal fibroblast cell lines IMR-90 and MRC-5 were purchased from ATCC and cultured at 37°C under 5% CO₂ using DMEM supplemented with 10% FBS and 100 u/ml-mg/ml penicillin-streptomycin. MSCs were provided by Dr. Michael Andreeff and cultured in α -MEM containing 10% FBS, 4% pooled human platelet lysate and 1% penicillin-streptomycin. Only third or fourth passage cells were used for experiments.

CTC Cell Culture—Cells were maintained at 37°C, 5% CO₂ under normoxic conditions. PDAC CTC-derived cell lines were grown in RPMI-1640 supplemented with 10% FBS and 1% antibiotic-antimycotic (Gibco).

Tissue slice culture—Fresh pancreatic cancer tissue samples were procured immediately after surgical resection from University of Michigan Hospital. Informed consent was obtained from all patients. The remaining connective, fibrotic or adipose tissue were removed with razor blades. Tumor specimens were embedded in 3% low melting point agarose/PBS before cutting in the Leica VT1200 tissue slicer. The slice thickness ranged between 100-200 μ m. Slices were then cultured in DMEM with penicillin (100 U/mL), streptomycin (100 U/mL) and amphotericin (Fungizone 2.5 μ g/mL). All experiments were performed in triplicate and were repeated at least three times.

CTC Isolation from Patient Blood and Healthy Controls

The experimental protocol was approved by the University of Michigan Medicine Institutional Review Board and all patients gave their informed consent to participate in the study. Patients were diagnosed with metastatic PDAC and were treatment naïve at the time of the first sample collection. Blood was collected in EDTA tubes and processed within two hours of sample collection. Red blood cells (RBCs) were depleted from the sample using RBC aggregation via HetaSep™ (STEMCELL Technologies) following the manufacturer's protocol. Briefly, blood was divided into 3 mL aliquots and mixed with 600 μ L HetaSep™, and centrifuged at 90xg for 1 minute, at room temperature, with the centrifuge brake off. The sample was then further incubated for an additional 10 minutes at room temperature to improve RBC depletion. The nucleated cell fraction was collected and diluted to 3x the original blood volume with phosphate buffered saline (PBS) (Gibco). The resultant sample was processed through the Labyrinth at a flowrate of 2500 μ L/min. The flow was stabilized for 1 mL of flow volume, before the CTC outlet, outlet 2, was collected, termed the CTC-enriched labyrinth product. This sample was divided for CTC enumeration (800 μ L) and RNA analysis (\approx 3-4 mL). Healthy control samples are the PBMCs that weren't depleted during our Labyrinth processing. Therefore, the data represents the background signal for gene expression in PBMCs and deviations from that are due to the presence of the CTCs in the patient samples.

Immunofluorescent Staining and CTC Enumeration

The CTC-enriched labyrinth product was divided across 4 Polysine microscope slides (Thermo Scientific), 200 μ L each, using Thermo Scientific™ Cytospin 4 (Thermo Scientific). The polysine slide were placed into an EZ Cytofunnel (Thermo scientific) and

spun at 800rpm for 10 minutes. To fix the cells, 200 μ L of 4% paraformaldehyde (PFA) was added to the Cytotunnel and spun a second time under the same conditions. Slides were stored at 4°C coated in PBS until used for immunofluorescent staining.

Slides were permeabilized with 0.2% Triton X-100 for 3 minutes, washed 3x with PBS, and blocked using 10% goat serum (Life Technologies) for 30 minutes at room temperature. The slides were then incubated overnight at 4°C with primary antibodies diluted in 10% goat serum - mouse anti-human Pan-Cytokeratin (CK) (Bio-Rad, MCA1907), mouse anti-human CD45 (Bio-Rad, MCA87GA), and rabbit anti-human Vimentin (Vim) (CST, 5741). The next day the slides were washed 3x with 5 minute incubation PBS washes. Slides were then incubated in the dark for 45 minutes at room temperature with secondary antibodies - (Alexa Fluor 488, 546, and 647). The slides were washed 3x with 5minute incubation PBS washes and mounted using Prolong Gold Antifade Mountant with DAPI (Invitrogen). The slides were scanned using a Nikon TI microscope at 20x magnification. The tiled images were individually analyzed, and CTC were identified based on their fluorescent signature in each channel.

Cells were considered CTCs when they were DAPI+/CD45 (AF 488)-/CK (AF 546)+. CTC phenotype was determined based on vimentin expression. Cells were considered epithelial if DAPI+/CD45 (AF 488)-/CK (AF 546)+/Vim (AF 647)-, and epithelial to mesenchymal transition (EMT) if DAPI+/CD45 (AF 488)-/CK (AF 546)+/Vim (AF 647)+.

Proliferation assay

Cells were cultured on 96-well plate in the indicated conditions. For cancer cells, cells growth was measured thereafter as fluorescence intensity using a plate reader (SpectraMax M5, Molecular Devices). For CAFs, CyQUANT® direct cell proliferation assay was performed according to the manufacturer's instructions.

Coculture assay with fibroblasts

Direct coculture in which two cell types were grown in physical contact was performed. In brief, CAFs or NOFs were seeded first and after the attachment, GFP labeled pancreatic cancer cells were seeded overnight. CAFs were maintained in complete media at least for 24h prior to changing to different media conditions. Fluorescence value as proliferation rates were measured at 485/515 nm or flow cytometry assay was performed.

Conditioned media (CM) preparation

PANC-1 cells were grown in DMEM + 10% FBS medium and conditioned medium was harvested after 16 h and centrifuged at 3,000 rpm for 5 min and supernatant was passed through 0.45- μ m filter. NOFs or MSCs were exposed to fresh CM repeatedly for 3 weeks.

Colony Formation Assay

Cell growth of shRNA-treated cell lines was assayed through crystal violet staining. 500 cells were seeded in 6-well plates. At the indicated time point (usually 2 weeks), cells were fixed with 80% methanol and stained with crystal violet solution overnight. All experiments were performed in triplicate.

Protein assay

Protein assays are used to do normalization in our experiment and is done according to Bicinchoninic Acid (BCA) Protein Assay protocol (Thermo Fisher). In brief, 200 μ l protein reagent was added to a 96-well assay plate and mix with samples or standard, and then incubated at 37°C for 30 min. The absorbance was read on a spectrophotometer at 562 nm and a standard curve was generated to determine sample protein concentration.

siRNA, shRNA and CRISPR knockdown

Cells were transfected with siBCAT1 (Sigma, EHU072291), siDBT (Sigma, EHU035851), siSMAD4 (Sigma, EHU149321), siSMAD5 (Sigma, EHU104241), siMRC2(Sigma, EHU003351) and respective negative controls (AM17011, Ambion; SIC001, Sigma) using Lipofectamine RNAiMAX Reagent (Thermo Fisher Scientific) and Opti-MEM accordingly to manufacturer's instructions and analysis was performed 3 days after transfection.

shRNA vectors were purchased from Sigma-Aldrich (St. Louis, USA). The clone IDs for each shRNA are as follows: shBCAT1-1: TRCN0000005907; shBCAT1-2: TRCN0000010976; shBCAT2-1: TRCN0000035115; shBCAT2-2: TRCN0000286266; shDBT-1: TRCN0000025837; shDBT-2: TRCN0000025838; A non-targeting shRNA (shCTRL) was used as a control. Knockdown was confirmed by qRT-PCR or immunoblotting.

For CRISPR knockdown of BCAT2, sgRNA oligonucleotide pairs (Pair1, CACCGCACGGATCATATGCTGACGG, AAACCCGTCAGCATATGATCCGTGC, Pair2, CACCGGTTACGGATCATATGCTGA, AAATCAGCATATGATCCGTGAACC were phosphorylated, annealed, and cloned as previously described into the BbsI-linearized pSpCas9(BB)-2A-Puro (PX459) V2.0 (PX459) plasmid (Addgene, #62988).

Quantitative RT-PCR

Total RNA was isolated using Trizol (Life Technologies) according to the manufacturer's instructions. RNA concentration was determined using a purified RNA by NanoDrop Lite Spectrophotometer (Thermo Fisher Scientific) and 1 μ g of cDNA synthesized using iScript cDNA synthesis kit (BioRad). Quantitative-RT PCR was performed using a QuantStudio 3 Real-Time PCR System (Applied Biosystems, Foster City, CA) with the Power SYBR™ Green PCR Master Mix (Invitrogen, Carlsbad, CA) as per the manufacturer's instructions. The primer sequences used for real-time qRT-PCR are the following: BCAT1 (Fwd GCCTTGGTGTGTGACAATGG, Rev CCATCACCCCTGATGTCTG), BCAT2 (Fwd AAATGGGCTGAGCTGATCC, Rev GAGTCATTGGTAGGGAGGCG), BCKDHA (Fwd GGAACGCCACTTCGTCATA, Rev GTGTGGCAGCGAAGTTGAAG), BCKDHB (Fwd TGGAGTCTTTAGATGCACTGTTG, Rev CGCAATTCGATTCCAAATCCAA), DBT (Fwd TTGCCTCCTTCACCCAAAGTT, Rev TGCCTGTGAATACCGGAGGT), SMAD2 (Fwd AACCTGCATTTTGGTGTTCGAT, Rev CCATCTACAGTGAGTGAGGGC), SMAD3 (Fwd AGCTGACACGGAGACACATC, Rev GTTGCATCCTGGTGGGATCT), SMAD4 (Fwd GAGACATACAGCACCCAGC, Rev TGTGGAAGCCACAGGAATGT), SMAD5 (Fwd ACAACACAGCCTTCTGGTTCA, Rev CGTGGCATTGTGGCATGT)

For the CTCs, the remainder of the CTC-enriched labyrinth product was centrifuged at 300xg for 10 minutes to pellet the cells. The cell pellet was resuspended in 700 μ L TRIzol to lyse the cells and incubated at room temperature for 5 minutes, and frozen at -20°C until ready for RNA purification. RNA was purified using a modified lysis protocol and the Total RNA Purification kit (Norgen Biotek Corp.). Once thawed, 140 μ L of chloroform was added to the TRIzol sample and centrifuged at 12,000xg for 15 minutes. The RNA layer was collected and mixed with equal volume 70% ethanol and loaded onto the spin column and washed 3x using the provided wash solution and eluted into 30 μ L volume. cDNA was prepared using SuperScript IV VILO with ezDNaseTM Enzyme (Invitrogen) following the manufacturer's protocol. Real-time PCR was performed using TaqManTM Fast Advanced Master Mix (Applied Biosystems) with following probes 18s:Hs99999901_s1, BCAT1:Hs00398962_m1, BCAT1:Hs01553550_m1, BCKDHA:Hs00958109_m1, BCKDHB:Hs00609053_m1, DBT:Hs01066445_m1 following the manufacturer's protocol and run on the QuantStudio 3. Detection thresholds were determined using the QuantStudioTM Design & Analysis Software.

Immunoblotting

Cells were washed twice in ice-cold phosphate-buffered saline (PBS), scraped and collected as pellets after centrifugation at 4,000 r.p.m. for 5 min. The pelleted cells were incubated in RIPA buffer with proteinase and phosphatase inhibitors for 15 min. Lysates were then collected and centrifuged at 14,000 r.p.m. for 15 min at 4°C . Protein concentrations were measured using the BCA Assay. SDS-PAGE and immunoblotting were performed in pre-cast bis-Tris 4-20% gradient gels (Bio-Rad). Blots were imaged using a ChemiDoc (Bio-Rad ChemiDocTM MP System). The following antibodies were used: BCAT1 (Novus Biologicals, NBP2-01826), BCAT2 (Cell Signaling Technologies (CST), 9432S), DBT (Abcam, ab151991), HSP90 (CST, 4877) and Vinculin (Santa Cruz Biotechnology, sc-25336).

Chromatin immunoprecipitation (ChIP) PCR

CAFs were treated with vehicle or 5 ng/ml TGF- β 1, then cross-linked, fixed and processed with Simple ChIP Enzymatic Chromatin IP Kit (Magnetic Beads) (CST, 9003) according to the manufacturer's instructions. Cell lysates were Immuno-precipitated with anti-SMAD4 antibody (CST, 38454), SMAD5 antibody (CST, 12534) and rabbit IgG ChIP grade (CST, 2729). Region of BCAT1 promoter or non-promoter region were amplified by Power SYBRTM Green PCR Master Mix (Invitrogen, Carlsbad, CA) as per the manufacturer's instructions.

Dual luciferase reporter assay

BCAT1 promoter regions were conjugated to the translation start site of the NanoLuc gene in the pNL2.1 vector (Promega). CAFs were plated in 96-well plates 12 h before transfection. The NanoLuc reporter vectors were co-transfected with promoter firefly luciferase reporter vector using Lipofectamine 3000 Reagent (Thermo) according to the manufacturer's protocol. After 48 h of the transfection, the luminescence was quantified and normalized using Nano-Glo Dual-Luciferase Reporter Assay (Promega).

Puromycin incorporation assay

Surface sensing of translation (SUnSET) assay was performed as previously described⁵¹. Briefly, cells were incubated with 10 μ g/mL puromycin (Thermo Fisher) for 10 min followed by washing with ice cold PBS and lysing with RIPA buffer. Cell lysates were loaded onto SDS-PAGE, and western blotting was performed with a mouse anti-puromycin monoclonal antibody (Millipore), and normalized against Ponceau S staining (Sigma).

Mitochondrial NADH/NAD⁺ measurement

Mitochondrial NADH/NAD⁺ sensor, RexMito, was prepared as previously described⁵². Mia Paca-2 cells were transfected using Lipofectamine 2000 Reagent (Thermo) according to the manufacturer's protocol. Then cell medium was replaced by complete medium, BCAA deprived medium or BCAA deprived medium with BCKA. We used a Nikon A1Si Laser Scanning Confocal Microscope to visualize the fluorescence of transfected cells 24-48 h after transfection. Fluorescence detection was carried out using 488 laser line for RexYFP and 561 laser line for HyPerRed-C199S. Imaging intensity was measured, and Ratio imaging were generated by Nikon NIS-Elements AR.

Flow Cytometry

In the mixed coculture, cancer associated fibroblasts were seeded in 6-well plate for 24 hours, For the SUnSET assay, then GFP labeled cells were added and cocultured for 3 days in the indicated medium. Puromycin intensity was analyzed by FACS in tumor cells with GFP gating. For the NADH/NAD⁺ measurement, PKH26 labeled cells were added and cocultured for 3 days in the indicated medium. NADH/NAD⁺ ratio was analyzed by FACS in tumor cells with PKH26 gating. All data were acquired with the Bio-Rad ZE5 flow cytometry analyzer and analysis were performed using FlowJo.

Measurements of OCR

Mitochondrial OCR was measured by XF96 Analyzer (Seahorse Biosciences). Cells were seeded in 96-well seahorse plates and incubated at 37 °C with 5% CO₂ overnight. Medium was replaced with 100 μ L medium free of serum and sodium bicarbonate. Plates were then incubated in CO₂-free incubator for 1 h before placing in an analyzer. The OCRs were measured with procedure of 3-min mixing, 2-min waiting and 3-min measuring. Oligomycin, FCCP and antimycin were injected through port A, B and C, respectively, to calculate mitochondrial function under different stress. All data were normalized to total cell protein as measured by the BCA assay.

Substrate specific OCR

OCR was measured in MAS medium supplemented with 0.2% (w/v) BSA, 4 mM ADP, 1 nM XF Plasma Membrane Permeabilizer (Seahorse Bioscience), 500 nM Coenzyme B12 and biotin and sequentially offered Oligomycin, FCCP and antimycin. Permeabilized pancreatic cancer cells were offered 5 mM branched chain ketoacids. Substrate specific respiration was calculated as the maximum respiration and the data were normalized to total cell protein.

Immunohistochemistry (IHC) and immunofluorescence (IF) staining

Tissues were fixed in 10% formalin overnight and embedded in paraffin. PDAC sections were deparaffinized in xylene, rehydrated through sequential ethanol, and rinsed in PBS. Non-specific signals were blocked using 10% goat serum in 0.1% Triton X-100. Tumor samples were stained with the following primary antibodies: α SMA(Sigma, A5228, 1:500), BCAT1 (Sigma, HPA048592, 1:200), SMAD5 (Sigma, HPA058931, 1:200), Ki-67(Santa Cruz Biotechnology,sc-239001:500), PCNA(Santa Cruz Biotechnology, sc-561:500). After overnight incubation, the slides were washed and incubated with biotinylated secondary antibody (Vector Laboratories) for 30min at room temperature. All slides were then incubated with avidin-biotin peroxidase complex for 30 min, and the signals were visualized by using DAB Substrate Kit (Vector Laboratories). The tissue sections were counterstained with VECTOR Hematoxylin QS and mounted with VectaMount after dehydration. IF staining was performed on tissue slices or chamber slide cultures (Thermo Fisher Scientific). The primary antibody was Anti-Proteasome 20S alpha + beta (Abcam, ab22673). Samples were mounted on microscope slides with Prolong Antifade with DAPI and imaged using a Nikon A1Si Laser Scanning Confocal Microscope.

BCAT activity assay

The enzymatic activity assay is performed as previously described⁵³. CAFs were homogenized in the buffer consisting of 20 mM EDTA, 20 mM EGTA, 0.4% (w/v) CHAPSO, 5 mM DTT, protease inhibitor cocktail, and 25 mM Hepes. The tissue homogenates were then frozen in a -80°C freezer for 1 h and then thawed at room temperature. The cellular debris was removed by centrifugation at 15,000g for 10 min at 4 $^{\circ}\text{C}$. The supernatant is then mixed with reaction buffer containing 10 mM L-leucine, 2 mM NAD⁺, and 100 mM sodium carbonate/bicarbonate buffer. The disappearance of absorbance at 340 nm due to NADH oxidation is measured continuously. BCAT activity is quantified by comparing the rate of loss of absorbance at 340 nm in the spectrophotometric assay mixture with or without bacterial leucine dehydrogenase or lacking bacterial leucine dehydrogenase.

Collagen Uptake

For the collagen uptake assays, cells were cultured with 25 $\mu\text{g}/\text{ml}$ Collagen for indicated periods of time in different medias. Subsequently, cells were washed 3 times with ice-cold PBS and fixed with 4% formaldehyde in PBS for 15 min. After fixation, cells were washed in PBS and mounted using Prolong Antifade + DAPI. To characterize internalization, confirm uptake and cleavage of ECM proteins by CAFs, we used fluorogenic DQ collagen (a self-quenched collagen that emits fluorescence upon degradation). For fluorescent staining, cells were incubated with FITC-collagen I for 48h and then stained with an antibody for the proteasome α and β subunits.

Proteasome Activity Assay

Proteasome activity was assessed by using the Cell-Based Proteasome-Glo Assay (Promega, G1180). Cells were trypsinized and plated according to the manufacturer's recommended instructions. Then cell medium was replaced by complete medium, BCAA-deprived medium

or medium with 5 ng/ml TGF- β . Luminescence was detected using SpectraMax M5 Microplate Reader (Molecular Devices) after 2 days.

Preparation of CAF-derived 3D ECMs

The cell derived ECMs were generated as previously described³⁰. Briefly, confluent CAF cultures were maintained for 7 days in the presence of daily added and freshly prepared ascorbic acid and ¹³C-labeled leucine, isoleucine and valine. Matrices were fixed or decellularized 7 days after plating. Cells were extracted from the matrices using 0.5% Triton X-100 (Sigma-Aldrich) and 20 mM NH₄OH. The matrices were washed in PBS three times and then treated with 10 U/ml DNase (Sigma-Aldrich) in DPBS for 30 minutes at 37°C. Labelled ECM was washed with PBS before plating CAFs, after 48 hours media was extracted for LC-MS. Decellularized ¹³C-BCAA-labeled ECM was obtained by culturing CAFs with ¹³C-labeled leucine, isoleucine, and valine for 8 days so that CAFs could incorporate labeled BCAAs into ECM protein. ECM internalization results were confirmed by measuring intracellular BCAA levels and ¹³C enrichment in CAFs cultured with ¹³C-BCAAs for 12 hours prior to deprivation. Intracellular BCAA levels were measured over 6, 12, 24, and 48 hours post-deprivation.

CTC derived organoid culture

To generate the CTC derived organoid, CAF were first seeded on CAF-derived 3D ECMs one day before. Then the fresh isolated CTC were seeded on the cultures. CTC derived Organoid was cultured as previously described without TGF- β modulators 5, it use Advanced DMEM F12 (Gibco) containing 1X antibiotic-antimycotic (Gibco) as base. Supplements include the following: N-acetyl-L-cysteine (NAC; Sigma-Aldrich), human gastrin 1 (Sigma-Aldrich), Gastrin I(Sigma-Aldrich), Nicotinamide (Sigma-Aldrich), R-spondin 1 (Peprotech), EGF(Peprotech) and FGF-10(Peprotech).

Scanning Electron Microscopy (SEM)

ECM were fixed in 2.5% glutaraldehyde in PBS at room temperature for one hour and then rinsed with PBS, followed by sequential dehydration with ethanol at concentrations of 50%, 70%, 90%, 95%, and 100% for 10 min each. The specimen was then immersed for 10 min in solution of 1:1 ethanol: hexamethyldisilazane (HMDS) and then transferred to 100% HMDS, followed by overnight air dry in the hood. The dehydrated specimen attached to carbon double sided tape are mounted on a SEM stub and coated with gold by sputtering. The ECM were examined by FEI Nova 200 Nanolab Dualbeam FIB scanning electron microscope under low beam energies (2.0-5.0 kV) at the Michigan Center for Materials Characterization (MC2) at University of Michigan.

Bioinformatics analysis of clinical data

Deconvolution and gene expression analysis: Data from real tumor samples available via the CBioPortal Database (most updated TCGA data for Pancreatic Ductal Adenocarcinoma patients) reflects the genomic and transcriptomic profile of a mixed population of cells in the TME. In order to compare the transcriptomic signatures of cancer cells and stromal cells (cancer-associated fibroblasts, CAFs) in the TCGA data we

developed a method to classify tumor samples as stromal-dominant and epithelial-dominant to represent CAFs and cancer cells. We used putative stromal and epithelial markers to cluster stromal- and epithelial-dominant samples. We performed k-means clustering using gene expression of 7 epithelial markers (CDH1, EPCAM, KRT7/8/10/18/19) and 46 myofibroblast markers (ACTA2, IL1R1, FAP, CCN2, ACTN1, CSF2RA, COL5A1, ITGB2, ITGAV, TIMP2, ADAM12, COL6A3, MMP9, FN1, PDGFC, COL1A2, COL6A2, FBN1, MMP2, MMP14, PLAU, PECAM1, CD93, CXCL12, SPRY1, ERG, ROBO4, TNXB, ACAN, CHI3L1, COL4A2, COMP, EFEMP2, FBLN1, FBLN2, FBN1, FBN2, IMPG2, ANOS1, LAMA4, LAMB1, LAMC1, MATN3, MFAP5, MGP, PRELP) to cluster samples into three or four clusters. The clustering on the tumor gene expression was performed to identify tumor samples that showed a dominant epithelial signature to represent cancer cell populations, and a dominant fibroblast signature to represent CAF cell populations. Since patient tumor samples are heterogeneous, containing cells other than malignant and CAF cells, we employ unsupervised k-means clustering based on epithelial and stromal markers alone. We account for “mixed” clusters, which represent samples that do not fall into either of the epithelial or stromal clusters. We tune the number of clusters, “k”, for the algorithm to pick out patient samples with distinct epithelial and CAF signatures. Performance of the k-means clustering is verified by assessing the distribution of samples with respect to their average stromal gene expression and average epithelial gene expression. Finally, expression of genes involved in branched-chain amino acid metabolism (BCAT1/2, BCKDHA/B, DBT and DLD) were compared across the clustered samples using a two-tailed t-test. ROBO1 expression was also compared across the clusters to independently validate the performance of clustering, since the ROBO1 gene is known to be highly expressed in stromal cells. The same methodology is employed for microarray data for PDAC tumor samples available from GSE21501, GSE36924 and GSE62165¹³⁻¹⁵, as well as RNASeq for healthy tissue (GTEx Analysis v8) from the GTEx Portal accessed on 08/29/2019. These studies were performed to discover molecular subtypes in patients with PDAC, which involved employing high-throughput transcriptomics analysis of tumor and normal tissue samples.

Differential expression from laser microdissected PDAC tumors: Raw counts of gene expression data were downloaded from GSE93326⁵⁴ and normalized using DESeq2. Normalized gene expression data was plotted to represent epithelial-stromal pairs obtained from the same tumor. Paired Wilcoxon t-test was used to estimate statistical significance of differential expression.

Single-cell gene expression analysis

CTC expression clustering: Gene expressions of branched-chain amino acid metabolism genes (BCAT1/2, BCKDHA and DBT) were measured in Day 0 CTCs and primary CAFs using qRT-PCR. Expression values of respective genes were normalized to gene expression measured in CAF1. Normalized expression values were converted to z-scores, followed by unsupervised hierarchical clustering.

PDAC single cell RNASeq (ScRNASeq) clustering: Pre-processed single-cell RNASeq data from two datasets published by Bernard et al¹⁸ and Peng et al¹⁹ were used in the analysis containing single-cell RNASeq data from two and 24 PDAC patients,

respectively. The data from Bernard et al was first filtered to remove outlier cells and only cells with total gene expression between 200 and 6100 UMI were retained for the downstream analysis. The filtered gene expression data for each cell was scaled and then log-normalized. Next, average expression of each gene across all cells was computed and the z-score of the dispersion of expressions from the mean was computed for each cell to identify genes that are differentially expressed across all cells. Principal component analysis (PCA) was then used to identify the most variable genes across all cells. An elbow plot of the PCA suggested the first twenty PCs were sufficient to capture most variance needed for the unsupervised clustering of the cell using a graph-based approach. The clusters generated were visualized using t-distributed Stochastic Neighbor Embedding (t-SNE) and identified using known cell type markers. All analyses were performed in R (v.3.5) following the Seurat (v 2.3.4) pipeline⁵⁵. The cluster information based on cell-type markers in the Peng et al study was used to generate a dotplot (Seurat v 2.3.4) for visualizing the differential gene expression of BCAA metabolism genes.

Metabolic flux analysis

Metabolite extraction for in vitro metabolomics and tracer studies: Cells cultured in 6-well plates were quenched with 800 μ L of ice-cold methanol/water (1:1) solution containing 1 μ g of Norvaline. Cells were scraped while keeping the plate on ice, followed by addition of 800 μ L of chloroform. The cell extracts were transferred to microcentrifuge tubes and vortexed for 30 minutes at 4 $^{\circ}$ C.

Metabolite extraction from tissue slices for metabolomics and tracer studies: Frozen tissue slices were transferred to Preceyllys CKMix Lysing tubes (Bertin Corp., 03961-1-009) and kept on dry ice. 200 μ L of ice-cold methanol/water (1:1) solution containing 1 μ g of Norvaline was added to the tubes to barely submerge the beads and tissue. The samples were homogenized using a Precellys Evolution Homogenizer with the Cryolys attachment to maintain the temperature below 4 $^{\circ}$ C in the homogenization chamber. Homogenization was achieved using two 30 second cycles at 6000 rpm with a pause of 60 seconds. Additional homogenization cycles were performed only when samples were not homogenized. Following homogenization, an additional 600 μ L of ice-cold methanol/water (1:1) solution was added to the tubes, as well as 800 μ L of chloroform. The homogenized extracts were transferred to microcentrifuge tubes and vortexed for 30 minutes at 4 $^{\circ}$ C.

Sample processing for polar metabolites, amino acid composition of proteins, and lipids: Metabolite extracts were centrifuged at 14,000g for 10 mins to separate the polar phase, protein interphase and chloroform phase. The water/methanol phase containing polar metabolites were transferred to fresh microcentrifuge tubes and dried in a SpeedVac and stored at -80° C until GC-MS analysis. Chloroform phase containing lipids were transferred to microcentrifuge tubes and dried under nitrogen and stored at -80° C. The protein layer was rinsed gently with chloroform, then PBS, and the liquid was discarded. The rinsed protein fractions were transferred to glass tubes with sealable caps and subjected to acid hydrolysis with 6M hydrochloric acid at 100 $^{\circ}$ C for 18-24 hours to obtain constituent amino acids. Hydrolyzed samples were dried under nitrogen and stored at -80° C until GC-MS analysis.

GC-MS Analysis for intracellular polar metabolites and amino acids from hydrolyzed protein: 30 μL of methoxyamine hydrochloride (MOX, Thermo Scientific) was added to dried samples and incubated at 30 $^{\circ}\text{C}$ for 2 hours with intermittent vortexing. 45 μL of MBTSTFA+1% TBDMCS was added to the samples and incubated at 55 $^{\circ}\text{C}$ for 1 hour. Derivatized samples were transferred to GC vials with glass inserts and added to the GC-MS autosampler queue. GC-MS analysis was performed using an Agilent 7890 GC equipped with a 30-m HP-5MSUI capillary column connected to an Agilent 5977B MS. For polar metabolites, the following heating cycle was used for the GC oven: 100 $^{\circ}\text{C}$ for three minutes, followed by a ramp of 5 $^{\circ}\text{C}/\text{min}$ to 300 $^{\circ}\text{C}$ and held at 300 $^{\circ}\text{C}$ for a total run time of 48 min. Data was acquired in scan mode. The relative abundance of metabolites was calculated from the integrated signal of all potentially labeled ions for each metabolite fragment. Mass Isotopologue Distributions (MID) were corrected for natural abundance using IsoCor prior to analysis with the model. Metabolite levels were normalized to internal standard Norvaline's signal and quantified using 6-point calibration with external standards for 19 polar metabolites.

LC-MS analysis to quantify BCKA secretion in media samples: Spent culture media samples were collected from culture plates and 200 μL was transferred to fresh microcentrifuge tubes for metabolic analysis. 800 μL of pre-chilled methanol was added to media samples and kept at -20 $^{\circ}\text{C}$ for 2 hours to deproteinize the samples. The samples were centrifuged at 14,000g for 10 minutes at 4 $^{\circ}\text{C}$, following which the supernatant was transferred to fresh tubes and dried in the SpeedVac. Media samples were derivatized with 500 μL of 12.5 mM OPD (o-phenylenediamine) solution in 2M hydrochloric acid. Samples were incubated at 80 $^{\circ}\text{C}$ for 20 minutes and transferred to an ice-bath to terminate the derivatization reaction. The derivatized solution was transferred to microcentrifuge tubes containing 0.08g of sodium sulfate. 500 μL of ethyl acetate was added to the samples, followed by vigorous vortexing and centrifuging at 1000g for 10 minutes. The ethyl acetate phase containing the derivatized ketoacids was transferred to fresh tubes and dried under nitrogen. The dried samples were reconstituted in 200 μL of 200 mM ammonium acetate solution and transferred to LC vials with glass inserts. The samples were analyzed with an Agilent Infinity LC stack using an Agilent Eclipse Plus C18 column (2.1 mm x 100 mm x 1.8 μm) connected to an Agilent 6520 QTOF. The following parameters were used for analysis, 5 mM ammonium acetate as Solvent A, methanol as solvent B, 380 $\mu\text{L}/\text{min}$ flow rate, 5-10 μL injection volume, 55% B for 4.2 minutes, ramp B to 95% for 0.9 minutes, retain 95% B for 1.5 minutes, return to initial conditions and equilibrate for 2.5 minutes. The analysis was performed in full-scan mode with the MS in positive ion mode.

Mole Percent Enrichment (MPE): MPE represents the fractional contribution of ^{13}C from a substrate to intermediate metabolite. It is calculated as follows, where N_C is the number of carbons that can be labeled as ^{13}C , and x_i is the fraction of $(M+i)^{\text{th}}$ isotopologue:

$$\text{MPE} = \left(\sum_{i=0}^{N_C} i * x_i \right) / N_C$$

Newly synthesized BCKA flux: To estimate *de novo* synthesized branched-chain ketoacid flux from 13-carbon labeled BCAA, we measure 13-carbon enrichment in respective branched-chain ketoacid much before cells reach isotopic steady-state:

$$\text{BCAA catabolic flux} = \frac{[(13\text{C mean enrichment})_{t=T} - (13\text{C mean enrichment})_{t=0}] * (\text{Intracellular abundance of BCKA})}{(\text{Total cell protein}) * (\text{Time to achieve } 13\text{C enrichment, } T)}$$

Statistics and Reproducibility

Data are presented as mean \pm s.d. All experiments were repeated twice with similar result unless otherwise stated. Graphpad Prism software V8.4 was used to conduct the statistical analysis of all data. Comparison of the data sets obtained from the different experiment conditions was performed with the two tailed student t test. Comparisons between multiple groups were made using one-way analysis of variance (ANOVA) with Tukey's post hoc comparison, and two-way ANOVA with Dunnett's post-testing for comparisons between multiple groups with independent variables. *P < 0.0001 unless otherwise stated.

DATA AVAILABILITY

The data that support the plots within this paper and other findings of this study are available from the corresponding author upon reasonable request. All requests should be directed to Deepak Nagrath, dnagrath@umich.edu.

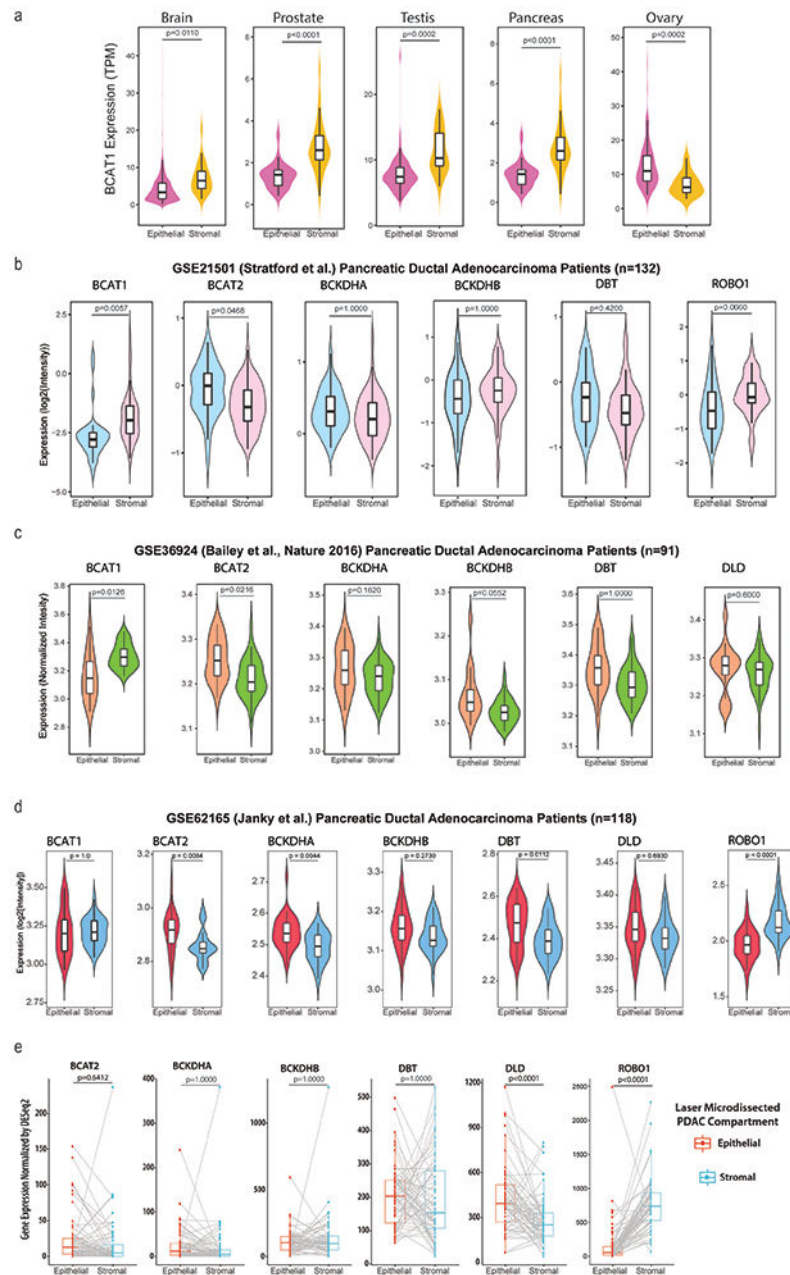
CODE AVAILABILITY

R code used for stromal/epithelial deconvolution, heat map generation, and violin plots and bioinformatics analysis is available from the corresponding author upon request.

Illustrations

Mitochondria used in the branched-chain amino acid metabolism schematic (Figure 1) was drawn using the PathWiz tool⁵⁶. The human body figure used in experimental schematics (Figure 6, Extended Data Figure 9) was obtained from the <https://www.freevectors.net/> database of free vector images.

Extended Data



Extended Data Fig. 1. Transcriptomic analysis of BCAA metabolic genes in PDAC tumors
a. Expression of BCAT1 healthy tissue samples from the GTEx database (Brain, n=2642; Prostate, n=245; Testis, n=361; Pancreas, n=328; Ovary, n=180). **b.** Expression of genes involved in BCAA metabolism in samples from GSE21501 (n=132). Tumor samples with dominant epithelial markers and dominant fibroblast markers are deconvolved to compare expression of metabolic genes between pancreatic cancer cells and stromal cells in the TME. ROBO1 is a marker for validation that has been found to be expressed in stromal cells but not in cancer cells in independent studies. **c.** Expression of genes involved in BCAA metabolism in samples from GSE36924 (n=91). **d.** Expression of genes involved in BCAA metabolism in samples from GSE62165 (n=118). Samples with dominant epithelial markers

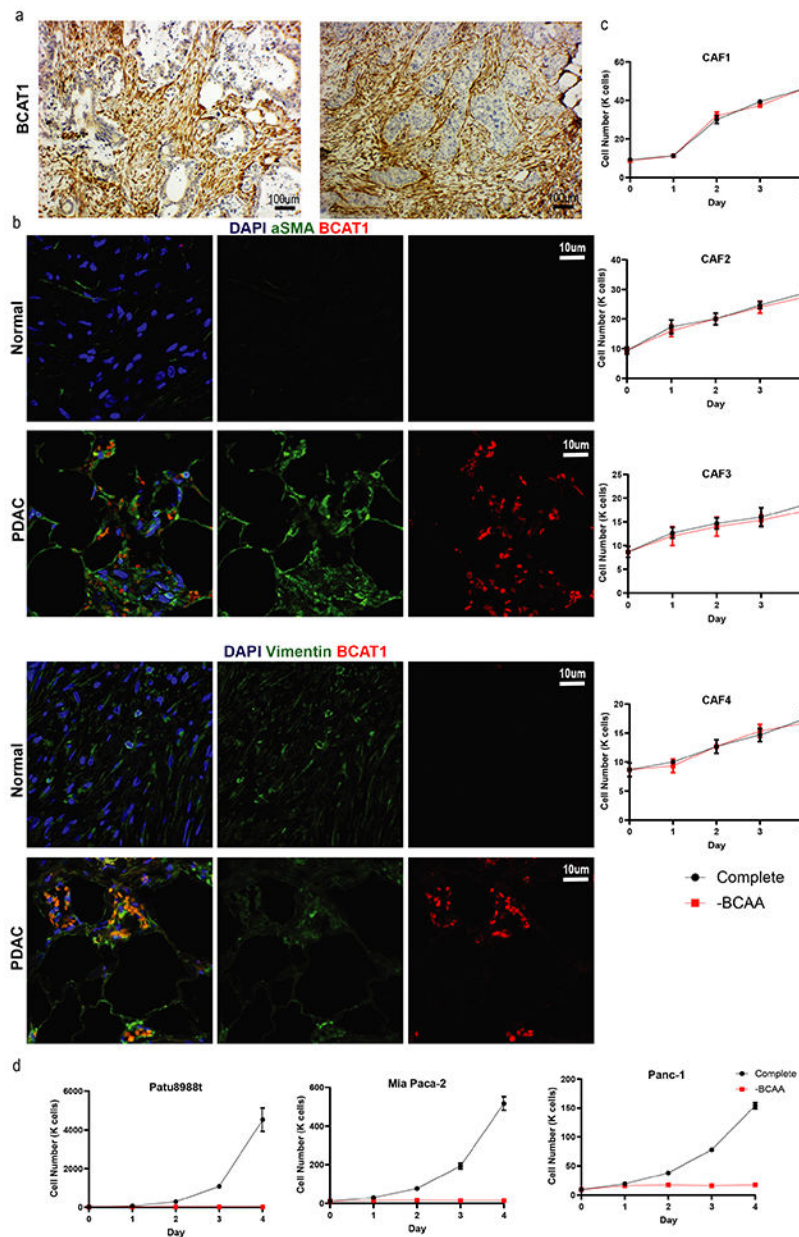
and dominant fibroblast markers are deconvolved to compare expression of metabolic genes between epithelial cells and stromal cells (a-d). **e.** Gene expression of BCAA pathway genes and ROBO1 in paired epithelial and stromal compartments obtained by laser microdissection (GSE 93326, n=63 paired samples). Violin plot represents all data points in each group (a-d). Boxplot limits represent median and interquartile range (IQR), and notches represent 1.5*IQR (a-e). Data analyzed using multiple, two-tailed, unpaired, Student's *t*-test (a-d); multiple, two-tailed, paired, Student's *t*-test (e).

Author Manuscript

Author Manuscript

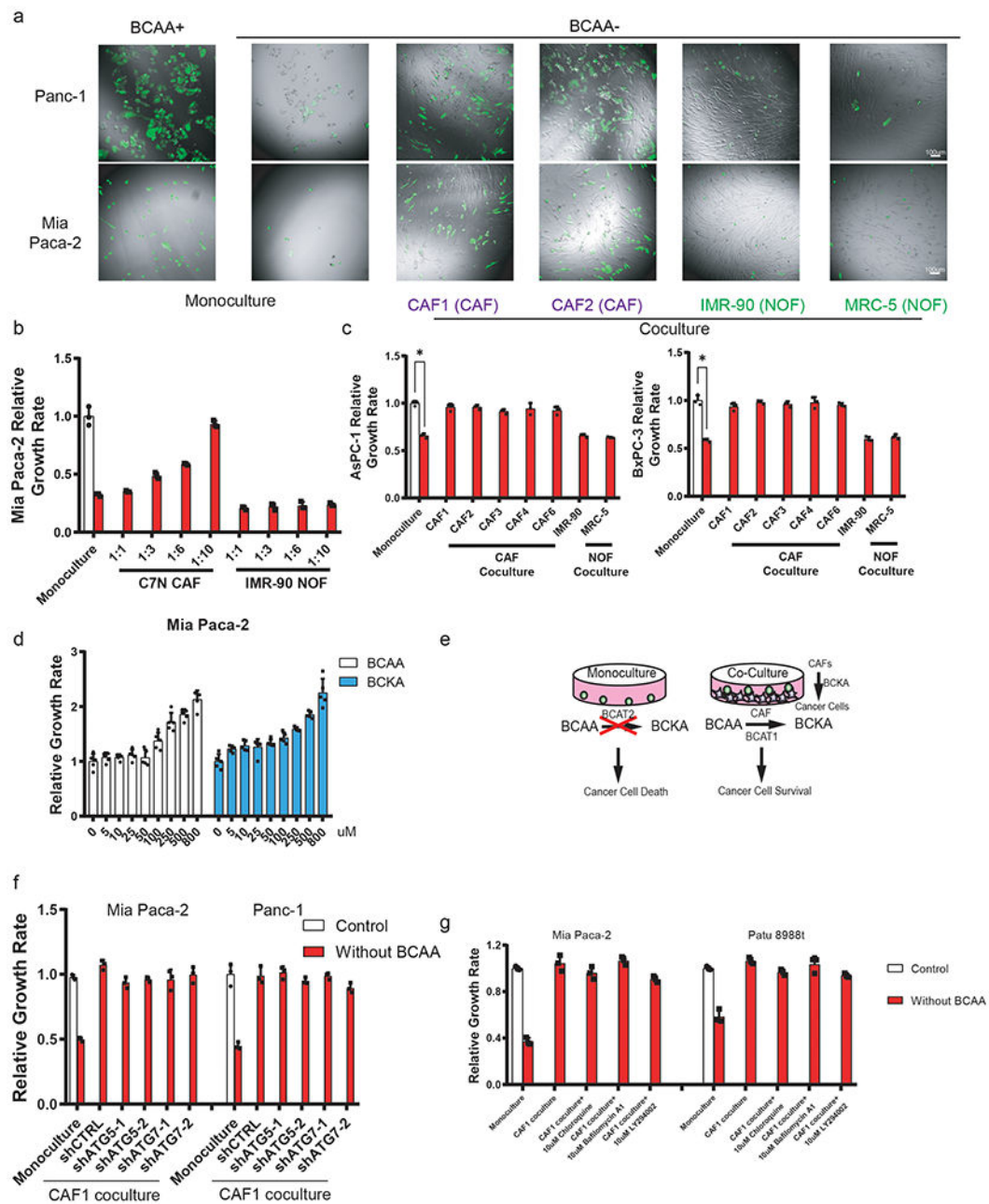
Author Manuscript

Author Manuscript



Extended Data Fig. 2. Characterization of BCAA metabolism

a. Representative IHC staining image comparing BCAT1 expression between stromal and tumor compartments. Experiments were repeated independently three times with similar results. **b.** Representative IF images showing protein expression of stromal α SMA, BCAT1 and Vimentin from paired healthy and PDAC tissue. Experiments were repeated independently three times with similar results. Experiments were repeated independently twice with similar results. **c.** Absolute cell numbers of PDAC CAFs were determined in the presence or absence of BCAA. $n = 3$ biologically independent samples. **d.** Absolute cell numbers of PDAC cell were determined in the presence or absence of BCAAs. $n = 3$ biologically independent samples. Data are presented as mean \pm s.d.



Extended Data Fig. 3. PDAC cells are BCAT2 dependent for growth

a. Fluorescence microscopy images merged with brightfield images comparing growth of GFP-labeled Mia Paca-2 and Panc-1 cells in contact co-cultures with CAFs or NOFs under BCAA deprivation. Experiments were repeated independently three times with similar results. **b.** Relative growth rates of Mia Paca-2 cells co-cultured with CAFs or NOFs at different seeding ratios under BCAA deprivation. $n = 3$ biologically independent samples. **c.** Relative growth rates of AsPC1 and BxPC-3 cells co-cultured with CAFs or NOFs under BCAA deprivation. $n = 3$ biologically independent samples. **d.** Relative growth rates of Mia Paca-2 cells in various concentrations of BCAAs or BCKAs. $n = 6$ biologically independent samples. **e.** Model for the rescue of proliferation in BCAT2 KD cancer cells by BCKAs

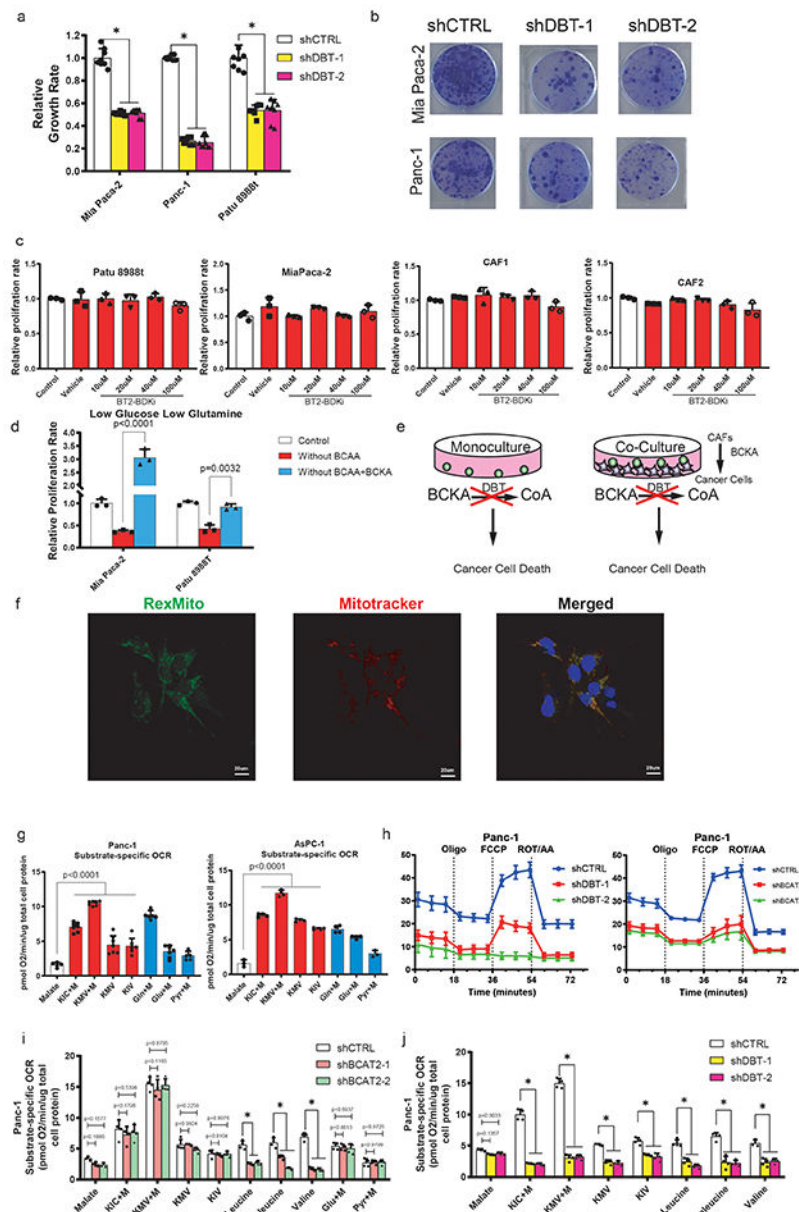
released from CAFs under BCAA deprivation. **f.** Relative growth rates of Mia Paca-2 and Panc-1 cells co-cultured with ATG-5/7 knockdown CAFs. n = 3 biologically independent samples. **g.** Relative growth rates of Mia Paca-2 and Patu 8988t cells cocultured with CAFs treated with autophagy inhibitors (chloroquine, Bafilomycin A1 and LY294002) under BCAA deprivation. n = 3 biologically independent samples. *P < 0.0001. Data are presented as mean \pm s.d. Two-tailed, unpaired, Student's *t*-test (c).

Author Manuscript

Author Manuscript

Author Manuscript

Author Manuscript



Extended Data Fig. 4. BCKDH complex is essential for PDAC cells growth and cell biosynthesis.
a. Relative proliferation rates of Mia Paca-2, Panc-1 and Patu 898t cells expressing control shRNA or two independent shRNAs to DBT. $n = 8$ biologically independent samples. **b.** Colony-formation assay of DBT knockdown pancreatic cell lines. $n = 3$ biologically independent samples. **c.** Relative growth rates of Patu 898t, Mia Paca-2 cells, and CAFs treated with BCKDK inhibitor, 3,6- dichlorobenzo[b]thiophene-2-carboxylic acid (BT2). $n = 3$ biologically independent samples. **d.** Relative growth rates of MiaPaca-2 and Patu 898t cells under BCAA deprivation and low glucose and low glutamine conditions after supplementation with BCKAs. $n = 3$ biologically independent samples. **e.** Schematic for the loss of rescue in DBT knockdown cancer cells by BCKAs released from CAFs under BCAA deprivation. **f.** Colocalization of Mitotracker and RexMito fluorescence in Mia Paca-2 cells.

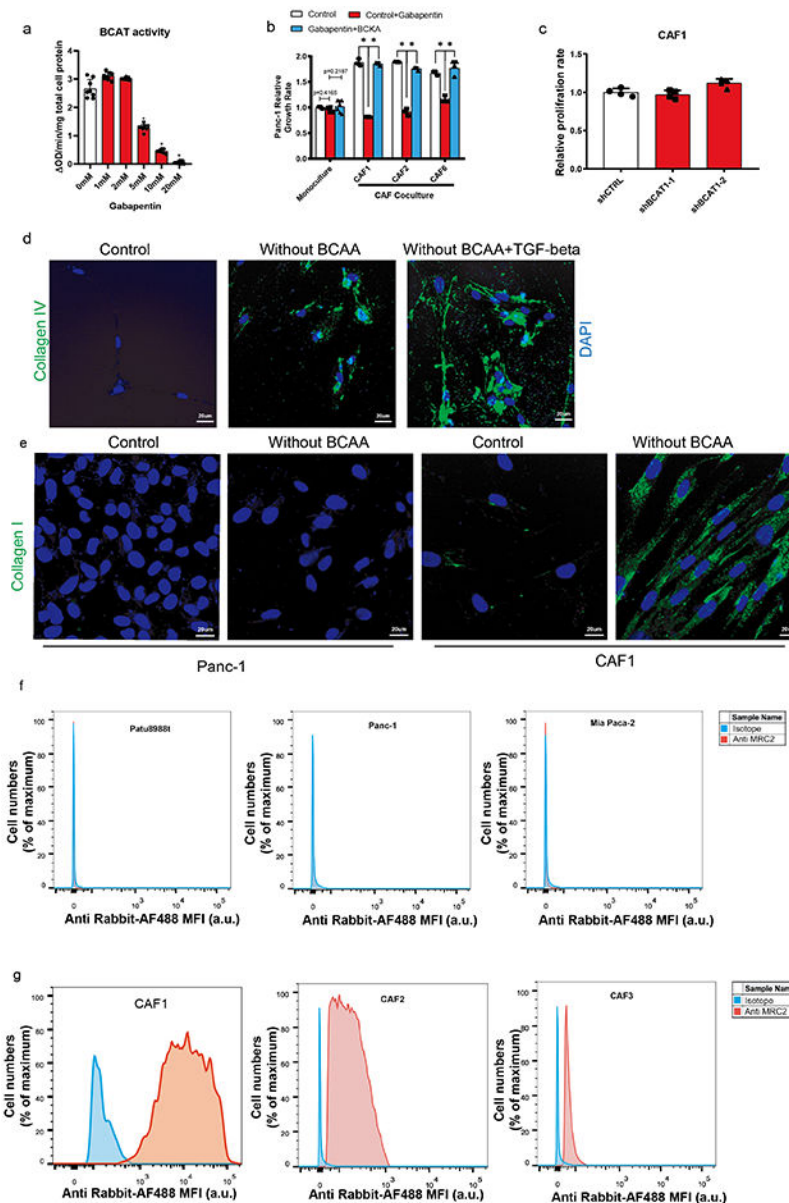
Mitotracker (red), RexMito (green), and DAPI (blue). Experiments were repeated independently three times with similar results. **g.** Substrate-specific oxygen consumption rate (OCR) in permeabilized pancreatic cancer cells. n = 4 biologically independent samples. **h.** OCR of Panc-1 cells after *BCAT2 and DBT* knockdown. n = 18 biologically independent samples. **i.** Substrate-specific OCR of *BCAT2* knockdown pancreatic cancer cells. n = 4 biologically independent samples. **j.** Substrate-specific of *DBT* knockdown pancreatic cancer cells. n = 4 biologically independent samples. *P < 0.0001. Data are presented as mean ± s.d. One-way ANOVA with Tukey's post hoc comparison (a,j); two-way ANOVA with Dunnett's multiple comparison test (i,j).

Author Manuscript

Author Manuscript

Author Manuscript

Author Manuscript



Extended Data Fig. 5. CAFs have upregulated collagen uptake under BCAA deprivation.
a. BCAT activity in CAFs treated with Gabapentin measured by spectrophotometric assay. $n = 6$ biologically independent samples. **b.** Growth rate of Panc-1 cancer cells with Gabapentin, BCKAs, and CAF coculture under BCAA deprivation **c.** The effect of knockdown of BCAT1 in CAFs on CAF growth rates. $n = 4$ biologically independent samples. **d.** Uptake of DQ-Collagen by CAFs after 24 h measured using confocal imaging. Experiments were repeated independently three times with similar results. **e.** Uptake of DQ-Collagen by PDAC cell lines and CAFs after 24 h measured using confocal imaging. Experiments were repeated independently three times with similar results. **f.** Flow cytometry assay of MRC2 expression in PDAC cell lines. Experiments were repeated independently three times with similar results. **g.** Flow cytometry assay of MRC2 expression in CAFs.

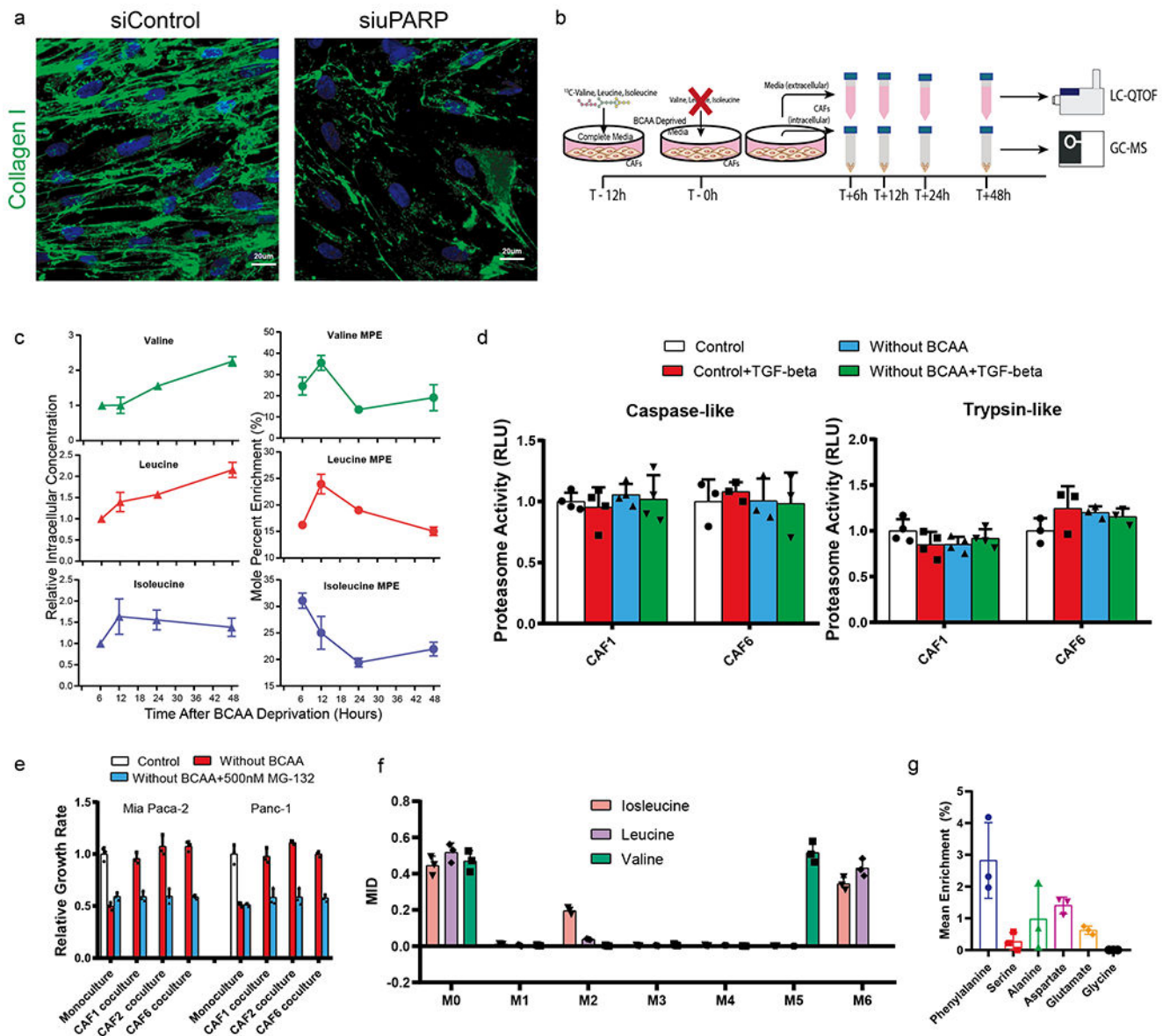
Experiments were repeated independently three times with similar results. * $P < 0.0001$. Data are presented as mean \pm s.d. One-way ANOVA with Tukey's post hoc comparison (b).

Author Manuscript

Author Manuscript

Author Manuscript

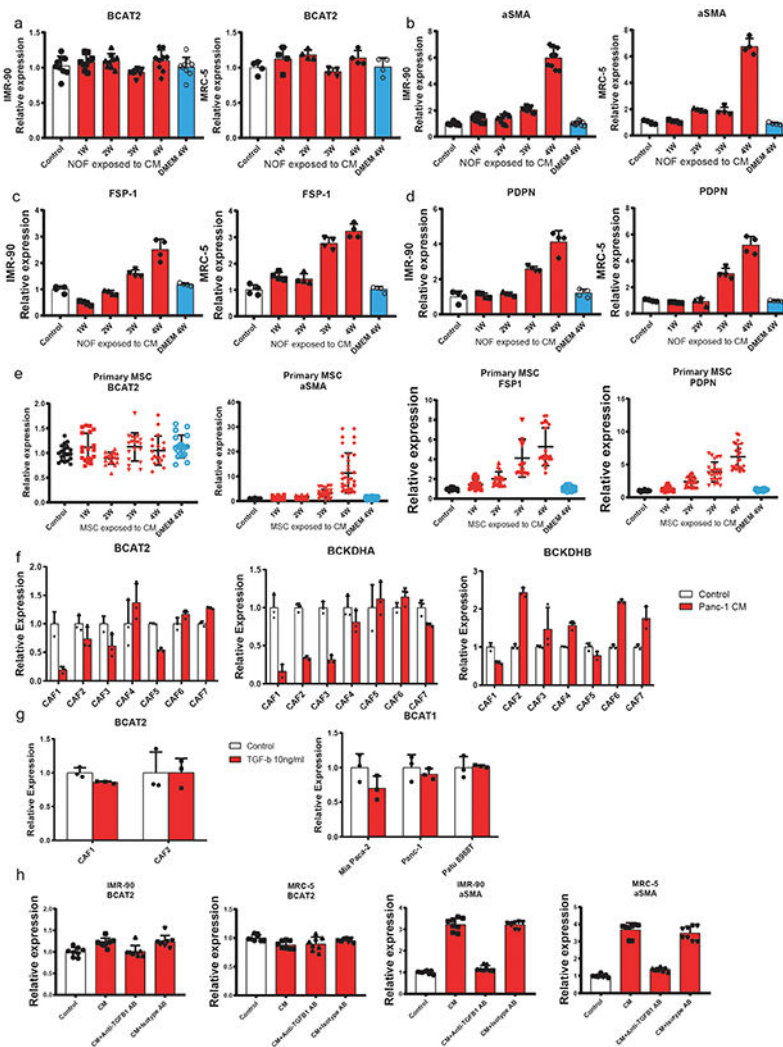
Author Manuscript



Extended Data Fig. 6. CAFs uptake collagen through the proteasome.

a. Uptake of DQ-Collagen by CAFs transfected with siControl or siuPARP measured using confocal imaging after 24 h. Experiments were repeated independently three times with similar results. **b.** CAFs are cultured with ^{13}C -BCAAs for 12 h prior to inducing BCAA deprivation. Spent media and cells are collected after 6, 12, 24, and 48 h under deprivation. Media samples are analyzed for secreted BCKAs using LC-QTOF and intracellular samples are analyzed for BCAAs using GC-MS. **c.** Intracellular BCAA levels measured after 6, 12, 24 and 48 h under BCAA deprivation. Mole percent enrichment of intracellular BCAAs measured after 6, 12, 24, and 48 h under BCAA deprivation. $n = 3$ biologically independent samples. **d.** Influence of TGF- β and BCAA deprivation on the proteasome activity in CAFs ($n=6$). **e.** Relative growth rates of Mia Paca-2 and Panc-1 cells cocultured with CAFs treated with MG-132 under BCAA deprivation conditions. $n = 8$ biologically independent samples.

f. Mass isotopomer distribution of BCAAs after acid hydrolysis of decellularized ECM proteins produced by CAFs cultured with ^{13}C -BCAAs. $n = 3$ biologically independent samples. **g.** Fractional enrichment of amino acids after acid hydrolysis of decellularized ECM proteins produced by CAFs cultured with ^{13}C -BCAAs. $n = 3$ biologically independent samples. Data are presented as mean \pm s.d.



Extended Data Fig. 7. Stromal BCAT1 is regulated by cancer-cell derived TGF- β .

a. BCAT2 expression in NOFs treated with pancreatic cancer cell conditioned media (CM). $n = 8$ biologically independent samples. **b.** α -smooth muscle actin, (α -SMA) expression in NOFs cultured with pancreatic cancer cell-CM over 4 weeks. $n = 8$ biologically independent samples. **c.** Fibroblast specific protein (FSP1) expression in NOFs cultured with pancreatic cancer cell-CM over 4 weeks. $n = 8$ biologically independent samples. **d.** Podoplanin (PDPN) expression in NOFs cultured with pancreatic cancer cell-CM over 4 weeks. $n = 8$ biologically independent samples. **e.** BCAT2, α -SMA, FSP-1 and PDPN expression in MSCs treated with pancreatic cancer cell CM. $n = 6$ biologically independent samples. **f.** Expression of BCAA related genes in CAFs treated with pancreatic cancer cell-CM. $n = 8$ biologically independent samples. **g.** BCAT2 expression in CAFs treated with TGF- β and BCAT1 expression in cancer cells treated with TGF- β . $n = 8$ biologically independent samples. **h.** BCAT2 and α -SMA expression in NOFs cultured with pancreatic cancer cell CM in presence of anti-TGF β 1 antibodies or isotype antibodies for 3 weeks. $n = 8$ biologically independent samples. Data are presented as mean \pm s.d.

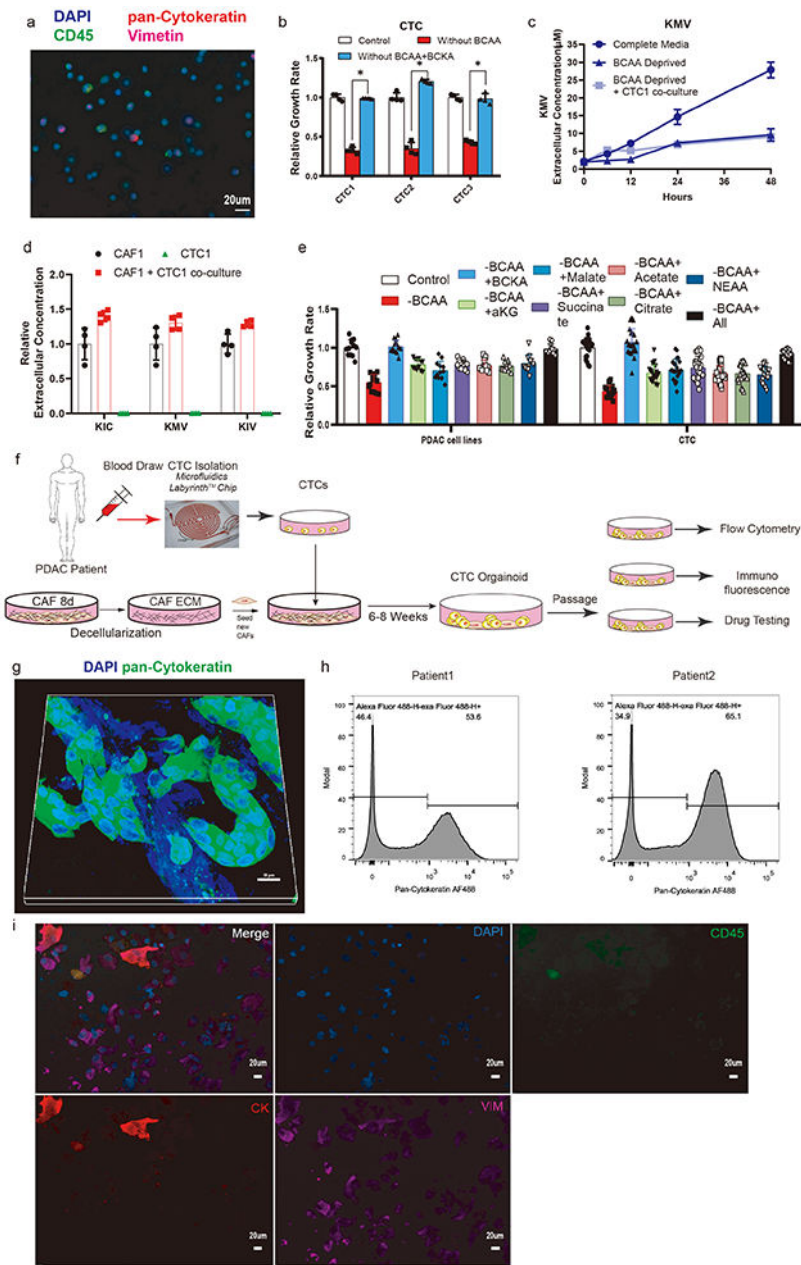
0.0001. Data are presented as mean \pm s.d. Multiple, two-tailed, unpaired, Student's *t*-test (b); one-way ANOVA with Tukey's post hoc comparison (c).

Author Manuscript

Author Manuscript

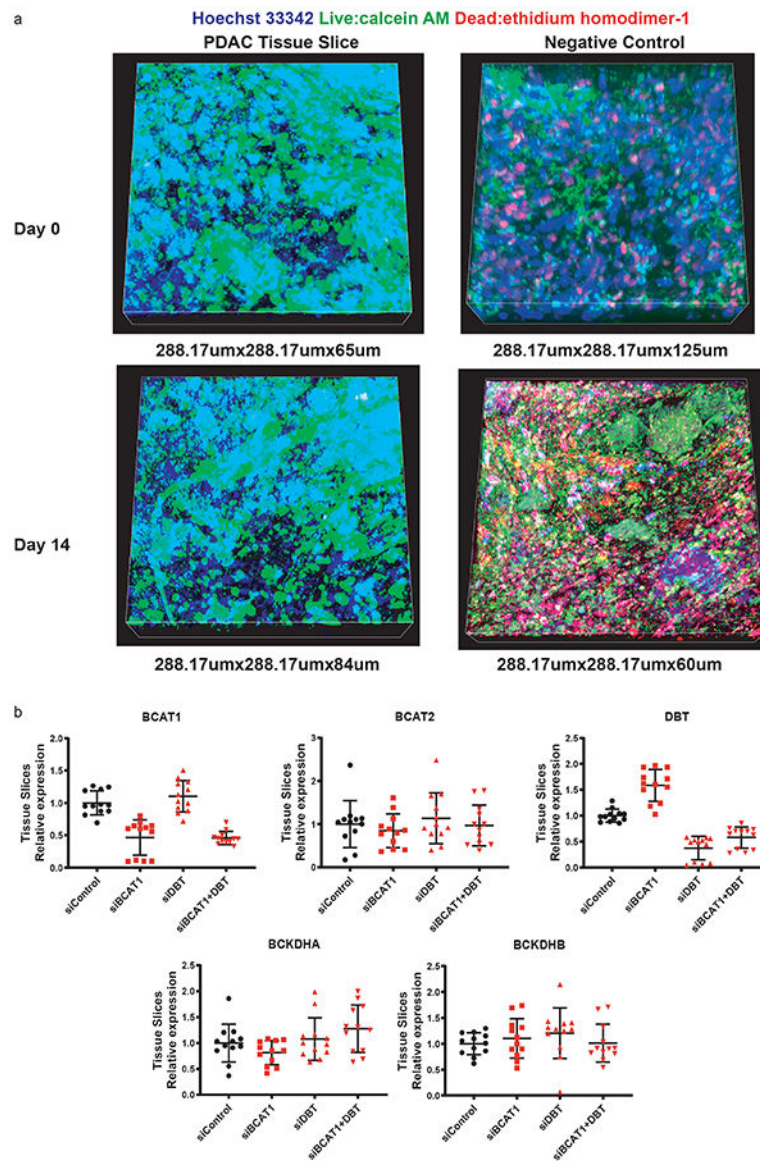
Author Manuscript

Author Manuscript



Extended Data Fig. 9. Validation of stromal BCAT1 and PDAC DBT in patient-derived CTCs.
a. Representative images of CTCs separated by Labyrinth. Cells are stained with DAPI (blue), cytokeratin (red), CD45 (green) and Vimentin (pink). Experiments were repeated independently three times with similar results. **b.** The influence of BCAAs and BCKAs on the growth of CTCs. $n = 8$ biologically independent samples. **c.** Extracellular concentration of BCKAs secreted by CAFs in monoculture and cocultured with CTCs over 6, 12, 24, and 48 h. $n = 3$ biologically independent samples. **d.** Extracellular concentration of BCKAs secreted by CAFs in monoculture or cocultured with CTCs, and CTCs in monoculture for 48 h. $n = 4$ biologically independent samples. **e.** Relative growth rate of PDAC cell lines and CTC lines under BCAA deprivation but supplemented with α KG, malate, succinate, acetate,

citrate, NEAA mixture, or a combination in BCAA-deprived media. **n** = 8 biologically independent samples. **f.** Schematic of the protocol used to generate CTC derived organoid with CAF secreted ECM. **g.** Representative images from a CTC-derived organoid. Cytokeratin is shown in green and the nuclei stained with DAPI are shown in blue. Experiments were repeated independently three times with similar results. **h.** Representative FACS data of Pan-Cytokeratin positive tumor cells in CTC derived organoids. Experiments were repeated independently three times with similar results. **i.** Representative images of CTC derived organoids. Cells are stained with DAPI (blue), cytokeratin (red), CD45 (green) and Vimentin (Pink). Experiments were repeated independently twice with similar results. * $P < 0.0001$. Data are presented as mean \pm s.d. Multiple, two-tailed, unpaired, Student's *t*-test (b).



Extended Data Fig. 10. Validation of stromal BCAT1 and PDAC DBT in patient-derived tissue slices.

a. Representative Live Dead assay of tissue slice at Day 0 and Day 14. Live cells fluoresce bright green, whereas dead cells fluoresce red. Positive controls were fixed by methanol. Experiments were repeated independently three times with similar results. **b.** Efficiency of BCAT1 and DBT siRNAs in the human PDAC tissue slices. Expression of BCAT1, BCAT2, DBT, BCKDHA and BCKDHB in the human PDAC tissue slices treated with BCAT1 and DBT siRNAs. $n = 6$ biologically independent samples. Data are presented as mean \pm s.d.

Supplementary Material

Refer to Web version on PubMed Central for supplementary material.

ACKNOWLEDGEMENTS

We truly thank and are grateful to three anonymous reviewers and editors for their incisive comments and several excellent suggestions. D.N. is supported by grants from NCI R01CA227622, R01CA222251, & R01CA204969. DN is also supported by Rogel Cancer Center grant. J.S. is supported by grant from NCI K08 CA234222. EC is funded by NCI grants R21CA231252 and R01CA232256, Core Grant CA06927. This work was supported in part by grants from NCI R01CA208335 to S.N. Flow cytometry experiments were performed in the Flow Cytometry Research Core at the University of Michigan, Biomedical Research Core Facilities (BRCF). Confocal microscopy was performed in the Microscopy and Image-analysis Laboratory (MIL) at the University of Michigan, Biomedical Research Core Facilities (BRCF).

References

1. Tonjes M et al. BCAT1 promotes cell proliferation through amino acid catabolism in gliomas carrying wild-type IDH1. *Nature medicine* 19, 901–908, doi:10.1038/nm.3217 (2013).
2. Raffel S et al. BCAT1 restricts α KG levels in AML stem cells leading to IDH mut-like DNA hypermethylation. *Nature* 551, 384 (2017). [PubMed: 29144447]
3. Green CR et al. Branched-chain amino acid catabolism fuels adipocyte differentiation and lipogenesis. *Nature chemical biology* 12, 15–21, doi:10.1038/nchembio.1961 (2016). [PubMed: 26571352]
4. Dey P et al. Genomic deletion of malic enzyme 2 confers collateral lethality in pancreatic cancer. *Nature* 542, 119–123, doi:10.1038/nature21052 (2017). [PubMed: 28099419]
5. Neesse A et al. Stromal biology and therapy in pancreatic cancer. *Gut* 60, 861, doi:10.1136/gut.2010.226092 (2011). [PubMed: 20966025]
6. Schworer S, Vardhana SA & Thompson CB Cancer Metabolism Drives a Stromal Regenerative Response. *Cell metabolism* 29, 576–591, doi:10.1016/j.cmet.2019.01.015 (2019). [PubMed: 30773467]
7. Neinast MD et al. Quantitative Analysis of the Whole-Body Metabolic Fate of Branched-Chain Amino Acids. *Cell metabolism* 29, 417–429 e414, doi:10.1016/j.cmet.2018.10.013 (2019). [PubMed: 30449684]
8. Mayers JR et al. Tissue of origin dictates branched-chain amino acid metabolism in mutant Kras-driven cancers. *Science (New York, N.Y.)* 353, 1161–1165, doi:10.1126/science.aaf5171 (2016).
9. Perera RM & Bardeesy N Pancreatic Cancer Metabolism: Breaking It Down to Build It Back Up. *Cancer discovery* 5, 1247–1261, doi:10.1158/2159-8290.Cd-15-0671 (2015). [PubMed: 26534901]
10. Danai LV et al. Altered exocrine function can drive adipose wasting in early pancreatic cancer. *Nature* 558, 600–604, doi:10.1038/s41586-018-0235-7 (2018). [PubMed: 29925948]
11. Uhlén M et al. Tissue-based map of the human proteome. *Science* 347, 1260419, doi:10.1126/science.1260419 (2015). [PubMed: 25613900]
12. Pinho AV et al. ROBO2 is a stroma suppressor gene in the pancreas and acts via TGF- β signalling. *Nature Communications* 9, 5083, doi:10.1038/s41467-018-07497-z (2018).
13. Bailey P et al. Genomic analyses identify molecular subtypes of pancreatic cancer. *Nature* 531, 47–52, doi:10.1038/nature16965 (2016). [PubMed: 26909576]
14. Janky R et al. Prognostic relevance of molecular subtypes and master regulators in pancreatic ductal adenocarcinoma. *BMC Cancer* 16, 632, doi:10.1186/s12885-016-2540-6 (2016). [PubMed: 27520560]
15. Stratford JK et al. A six-gene signature predicts survival of patients with localized pancreatic ductal adenocarcinoma. *PLoS medicine* 7, e1000307, doi:10.1371/journal.pmed.1000307 (2010). [PubMed: 20644708]
16. Neesse A, Algul H, Tuveson DA & Gress TM Stromal biology and therapy in pancreatic cancer: a changing paradigm. *Gut* 64, 1476–1484, doi:10.1136/gutjnl-2015-309304 (2015). [PubMed: 25994217]
17. Zhao H et al. Tumor microenvironment derived exosomes pleiotropically modulate cancer cell metabolism. *eLife* 5, e10250, doi:10.7554/eLife.10250 (2016). [PubMed: 26920219]
18. Bernard V et al. Single-Cell Transcriptomics of Pancreatic Cancer Precursors Demonstrates Epithelial and Microenvironmental Heterogeneity as an Early Event in Neoplastic Progression.

- Clinical cancer research : an official journal of the American Association for Cancer Research 25, 2194–2205, doi:10.1158/1078-0432.Ccr-18-1955 (2019). [PubMed: 30385653]
19. Peng J et al. Single-cell RNA-seq highlights intra-tumoral heterogeneity and malignant progression in pancreatic ductal adenocarcinoma. *Cell Research* 29, 725–738, doi:10.1038/s41422-019-0195-y (2019). [PubMed: 31273297]
 20. Sousa CM et al. Pancreatic stellate cells support tumour metabolism through autophagic alanine secretion. *Nature* 536, 479–483, doi:10.1038/nature19084 (2016). [PubMed: 27509858]
 21. Lu G et al. Protein phosphatase 2Cm is a critical regulator of branched-chain amino acid catabolism in mice and cultured cells. *The Journal of Clinical Investigation* 119, 1678–1687, doi:10.1172/JCI38151 (2009). [PubMed: 19411760]
 22. Grankvist N, Lagerborg KA, Jain M & Nilsson R Gabapentin Can Suppress Cell Proliferation Independent of the Cytosolic Branched-Chain Amino Acid Transferase 1 (BCAT1). *Biochemistry* 57, 6762–6766, doi:10.1021/acs.biochem.8b01031 (2018). [PubMed: 30427175]
 23. Sherman MH et al. Vitamin D receptor-mediated stromal reprogramming suppresses pancreatitis and enhances pancreatic cancer therapy. *Cell* 159, 80–93, doi:10.1016/j.cell.2014.08.007 (2014). [PubMed: 25259922]
 24. Sherman MH et al. Stromal cues regulate the pancreatic cancer epigenome and metabolome. *Proceedings of the National Academy of Sciences of the United States of America* 114, 1129–1134, doi:10.1073/pnas.1620164114 (2017). [PubMed: 28096419]
 25. Commisso C et al. Macropinocytosis of protein is an amino acid supply route in Ras-transformed cells. *Nature* 497, 633–637, doi:10.1038/nature12138 (2013). [PubMed: 23665962]
 26. Madsen DH et al. The non-phagocytic route of collagen uptake: a distinct degradation pathway. *J Biol Chem* 286, 26996–27010, doi:10.1074/jbc.M110.208033 (2011). [PubMed: 21652704]
 27. Jurgensen HJ et al. Immune regulation by fibroblasts in tissue injury depends on uPARAP-mediated uptake of collectins. *The Journal of cell biology* 218, 333–349, doi:10.1083/jcb.201802148 (2019). [PubMed: 30366943]
 28. Mishra PJ et al. Carcinoma-associated fibroblast-like differentiation of human mesenchymal stem cells. *Cancer research* 68, 4331–4339, doi:10.1158/0008-5472.CAN-08-0943 (2008). [PubMed: 18519693]
 29. Yeung TL et al. TGF-beta modulates ovarian cancer invasion by upregulating CAF-derived versican in the tumor microenvironment. *Cancer research* 73, 5016–5028, doi:10.1158/0008-5472.CAN-13-0023 (2013). [PubMed: 23824740]
 30. Franco-Barraza J et al. Matrix-regulated integrin alphavbeta5 maintains alpha5beta1-dependent desmoplastic traits prognostic of neoplastic recurrence. *Elife* 6, doi:10.7554/eLife.20600 (2017).
 31. Ashworth T A case of cancer in which cells similar to those in the tumours were seen in the blood after death. *Aust Med J* 14, 146–149 (1869).
 32. Allard WJ et al. Tumor cells circulate in the peripheral blood of all major carcinomas but not in healthy subjects or patients with nonmalignant diseases. *Clin Cancer Res* 10, 6897–6904 (2004). [PubMed: 15501967]
 33. Nagrath S, Jack RM, Sahai V & Simeone DM Opportunities and Challenges for Pancreatic Circulating Tumor Cells. *Gastroenterology* 151, 412–426, doi:10.1053/j.gastro.2016.05.052 (2016). [PubMed: 27339829]
 34. Lin E et al. High-Throughput Microfluidic Labyrinth for the Label-free Isolation of Circulating Tumor Cells. *Cell Syst* 5, 295–304 e294, doi:10.1016/j.cels.2017.08.012 (2017). [PubMed: 28941584]
 35. Rivera-Baez L et al. Expansion of Circulating Tumor Cells from Patients with Locally Advanced Pancreatic Cancer Enable Patient Derived Xenografts and Functional Studies for Personalized Medicine. *Cancers (Basel)* 12, doi:10.3390/cancers12041011 (2020).
 36. van Geer MA et al. Ex-vivo evaluation of gene therapy vectors in human pancreatic (cancer) tissue slices. *World journal of gastroenterology* 15, 1359–1366, doi:10.3748/wjg.15.1359 (2009). [PubMed: 19294766]
 37. Roife D et al. Ex Vivo Testing of Patient-Derived Xenografts Mirrors the Clinical Outcome of Patients with Pancreatic Ductal Adenocarcinoma. *Clinical cancer research : an official journal of*

- the American Association for Cancer Research 22, 6021–6030, doi:10.1158/1078-0432.CCR-15-2936 (2016). [PubMed: 27259561]
38. Auciello FR et al. A Stromal Lysolipid-Autotaxin Signaling Axis Promotes Pancreatic Tumor Progression. *Cancer discovery* 9, 617–627, doi:10.1158/2159-8290.CD-18-1212 (2019). [PubMed: 30837243]
 39. Kamphorst JJ et al. Human pancreatic cancer tumors are nutrient poor and tumor cells actively scavenge extracellular protein. *Cancer Res* 75, 544–553, doi:10.1158/0008-5472.CAN-14-2211 (2015). [PubMed: 25644265]
 40. Halbrook CJ et al. Macrophage-Released Pyrimidines Inhibit Gemcitabine Therapy in Pancreatic Cancer. *Cell metabolism* 29, 1390–1399.e1396, doi:10.1016/j.cmet.2019.02.001 (2019). [PubMed: 30827862]
 41. Dalin S et al. Deoxycytidine Release from Pancreatic Stellate Cells Promotes Gemcitabine Resistance. *Cancer Res* 79, 5723–5733, doi:10.1158/0008-5472.CAN-19-0960 (2019). [PubMed: 31484670]
 42. Li JT et al. BCAT2-mediated BCAA catabolism is critical for development of pancreatic ductal adenocarcinoma. *Nature cell biology* 22, 167–174, doi:10.1038/s41556-019-0455-6 (2020). [PubMed: 32029896]
 43. Lee JH et al. Branched-chain amino acids sustain pancreatic cancer growth by regulating lipid metabolism. *Exp Mol Med* 51, 1–11, doi:10.1038/s12276-019-0350-z (2019).
 44. Ohlund D et al. Distinct populations of inflammatory fibroblasts and myofibroblasts in pancreatic cancer. *The Journal of experimental medicine* 214, 579–596, doi:10.1084/jem.20162024 (2017). [PubMed: 28232471]
 45. Biffi G et al. IL1-Induced JAK/STAT Signaling Is Antagonized by TGFbeta to Shape CAF Heterogeneity in Pancreatic Ductal Adenocarcinoma. *Cancer discovery* 9, 282–301, doi:10.1158/2159-8290.Cd-18-0710 (2019). [PubMed: 30366930]
 46. Elyada E et al. Cross-Species Single-Cell Analysis of Pancreatic Ductal Adenocarcinoma Reveals Antigen-Presenting Cancer-Associated Fibroblasts. *Cancer discovery* 9, 1102–1123, doi:10.1158/2159-8290.Cd-19-0094 (2019). [PubMed: 31197017]
 47. Mishra R, Haldar S, Suchanti S & Bhowmick NA Epigenetic changes in fibroblasts drive cancer metabolism and differentiation. *Endocr Relat Cancer* 26, R673–R688, doi:10.1530/ERC-19-0347 (2019). [PubMed: 31627186]
 48. Bhagat TD et al. Lactate-mediated epigenetic reprogramming regulates formation of human pancreatic cancer-associated fibroblasts. *eLife* 8, e50663, doi:10.7554/eLife.50663 (2019). [PubMed: 31663852]
 49. Olivares O et al. Collagen-derived proline promotes pancreatic ductal adenocarcinoma cell survival under nutrient limited conditions. *Nat Commun* 8, 16031, doi:10.1038/ncomms16031 (2017). [PubMed: 28685754]
 50. Sprangers S, Behrendt N, Engelholm L, Cao Y & Everts V Phagocytosis of Collagen Fibrils by Fibroblasts In Vivo Is Independent of the uPARAP/Endo180 Receptor. *J Cell Biochem* 118, 1590–1595, doi:10.1002/jcb.25821 (2017). [PubMed: 27922193]

Methods-only References

51. Schmidt EK, Clavarino G, Ceppi M & Pierre P SUnSET, a nonradioactive method to monitor protein synthesis. *Nature methods* 6, 275–277, doi:10.1038/nmeth.1314 (2009). [PubMed: 19305406]
52. Bilan DS et al. Genetically encoded fluorescent indicator for imaging NAD(+)/NADH ratio changes in different cellular compartments. *Biochimica et biophysica acta* 1840, 951–957, doi:10.1016/j.bbagen.2013.11.018 (2014). [PubMed: 24286672]
53. Cooper AJ, Conway M & Hutson SM A continuous 96-well plate spectrophotometric assay for branched-chain amino acid aminotransferases. *Anal Biochem* 308, 100–105, doi:10.1016/s0003-2697(02)00243-9 (2002). [PubMed: 12234469]

54. Maurer C et al. Experimental microdissection enables functional harmonisation of pancreatic cancer subtypes. *Gut* 68, 1034–1043, doi:10.1136/gutjnl-2018-317706 (2019). [PubMed: 30658994]
55. Butler A, Hoffman P, Smibert P, Papalexi E & Satija R Integrating single-cell transcriptomic data across different conditions, technologies, and species. *Nature Biotechnology* 36, 411, doi:10.1038/nbt.4096 (2018).
56. Pon A et al. Pathways with PathWhiz. *Nucleic acids research* 43, W552–559, doi:10.1093/nar/gkv399 (2015). [PubMed: 25934797]

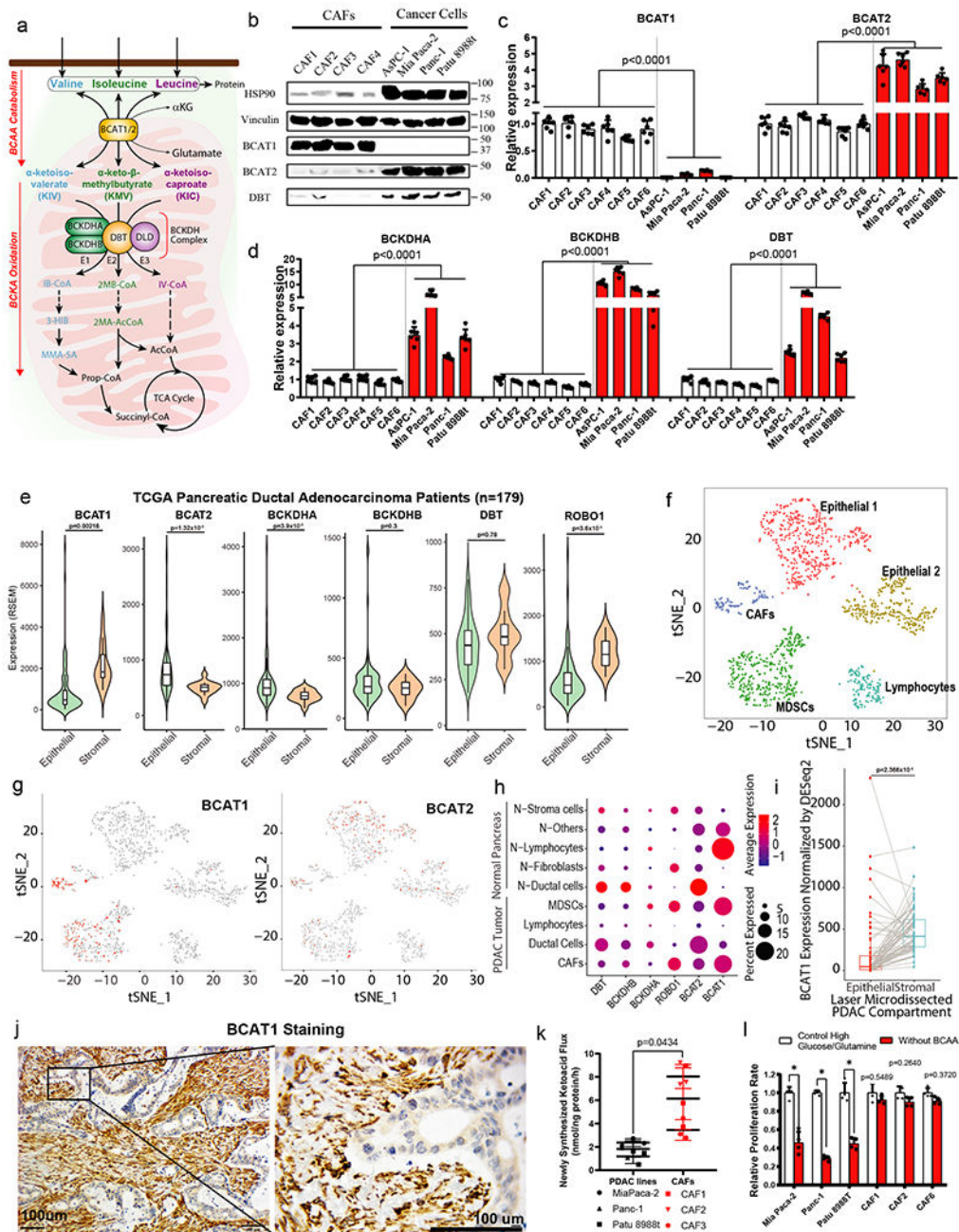


Fig. 1. Characterization of BCAA metabolism in CAFs and cancer cells.

a. BCAA transaminases (BCAT1/2), deaminate BCAAs to branched chain α-ketoacids (BCKAs), α-ketoisovalerate (KIV), α-keto-β-methylbutyrate (KMV), and α-ketoisocaproate (KIC). Then the mitochondrial BCKA dehydrogenase (BCKDH) complex consisting of three catalytic components, α-ketoacid dehydrogenase (E1), dihydrolipoyltransacylase (E2), and dihydrolipoamide dehydrogenase (E3) irreversibly oxidizes BCKAs. **b.** Immunoblots of BCAT1, BCAT2 and DBT expression in CAFs and pancreatic cancer cell lines. HSP90 and Vinculin used as loading control. Experiments were repeated independently three times with similar results. **c.** Relative BCAT1/2 mRNA

expression in CAFs and PDAC lines, normalized to gene expression in CAF1. $n = 4$ biologically independent samples. **d.** Relative BCKDHA, BCKDHB, and DBT mRNA expression determined by qRT-PCR in CAFs and pancreatic cancer cell lines. Expression normalized to gene expression in CAF1. $n = 4$ biologically independent samples. **e.** Expression of genes in BCAA metabolism in samples from TCGA PDAC dataset ($n=179$). Violin plot represents all samples in each group. **f.** t-SNE clustering of single-cell gene expression of PDAC tumor cells ($n=1352$ single cells from $N=2$ patient samples). **g.** BCAT1 is predominantly expressed in single cells identified as CAFs, while BCAT2 is primarily expressed in single cells identified as PDAC cells. **h.** Single-cell gene expression of BCAA metabolic genes from $N=24$ PDAC tumor samples ($n=41986$ single cells) and $N=11$ healthy pancreatic tissue samples ($n=15544$ single cells) by t-SNE-clustered cell-types. **i.** BCAT1 gene expression in paired epithelial and stromal compartments obtained by laser microdissection of human PDAC tumors (GSE93326, $n=63$ paired samples). **j.** Representative IHC staining comparing BCAT1 expression between stromal and tumor compartments. Experiments were repeated independently three times with similar results. **k.** Newly synthesized BCKA flux determined by ^{13}C -BCAA tracing in PDAC cells and CAFs. $n = 3$ biologically independent samples. **l.** Relative proliferation rates of Mia Paca-2, Panc-1 and Patu 8988t pancreatic cancer cells or CAFs under BCAA deprivation. $n = 4$ biologically independent samples. $*P < 0.0001$. Data are presented as mean \pm s.d. One-way ANOVA with Tukey's post hoc comparison (a); two-tailed, paired, Student's t -test (i); multiple, two-tailed, unpaired, Student's t -test (e, k). Boxplot limits represent median and interquartile range (IQR), and notches represent $1.5 \times \text{IQR}$ (e,i).

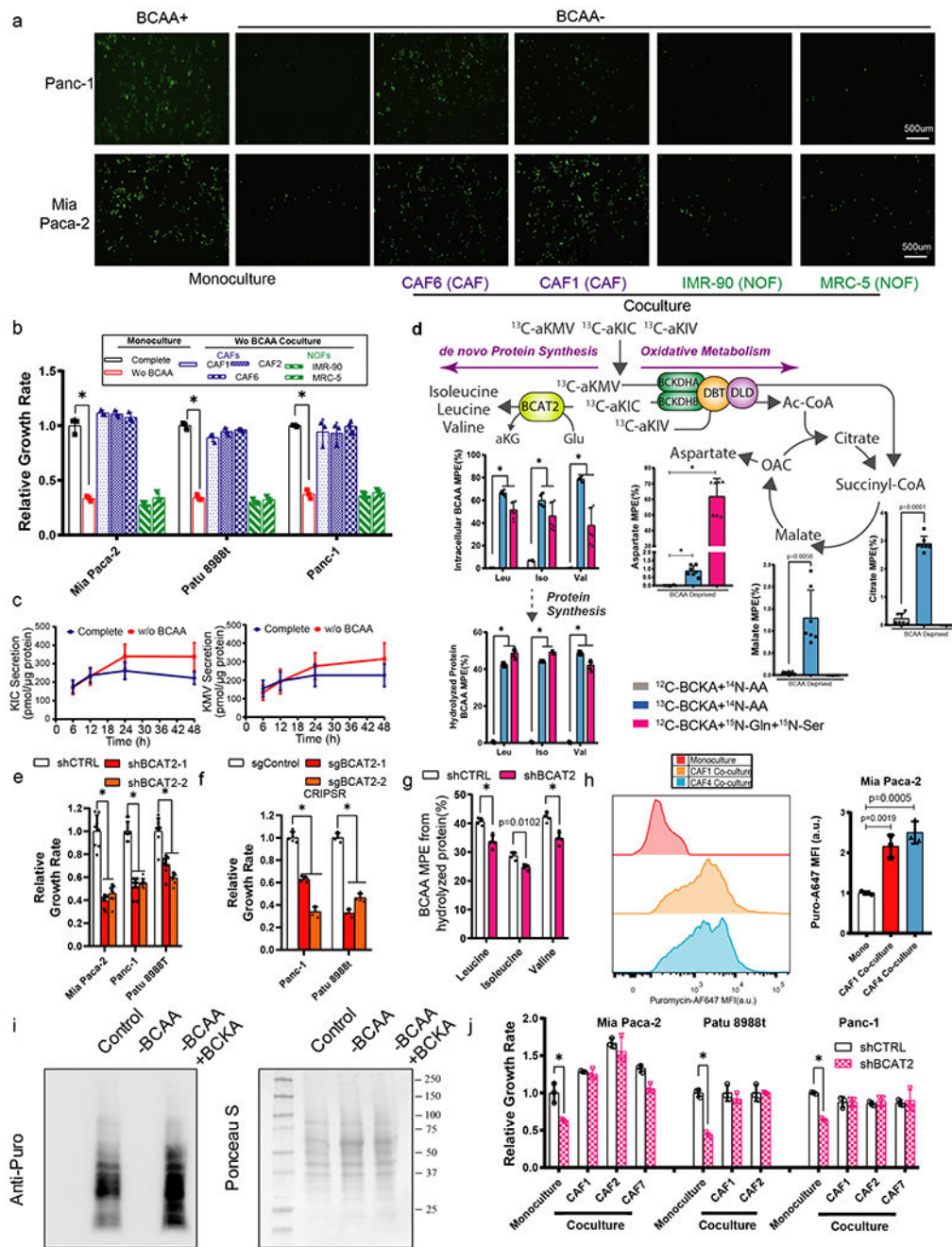


Fig. 2. PDAC cells are BCAT2 dependent for growth and respiration.

a. Fluorescence microscopy images comparing growth of GFP-labeled Mia Paca-2 and Panc-1 cells in contact co-cultures with CAFs or NOFs under BCAA deprivation. Experiments were repeated independently three times with similar results. **b.** Relative proliferation rates of Mia Paca-2, Patu 8988t and Panc-1 pancreatic cancer cells under BCAA deprivation. $n = 3$ biologically independent samples. **c.** BCKA secretion by CAFs estimated by measuring extracellular concentration of BCKAs, KIC and KMV, at 6, 12, 24, and 48h by LC-MS. $n = 3$ biologically independent samples. **d.** Fate of ¹³C-BCKAs in PDAC cells elucidated by measuring mole percent enrichment (MPE) of TCA cycle

intermediates that represent BCKA oxidation, and of intracellular BCAAs and BCAAs from acid-hydrolyzed proteins that represent *de novo* protein synthesis. **n** = 7 biologically independent samples for intracellular metabolites and **n** = 4 biologically independent samples for protein hydrolyzed metabolites. **e.** Relative proliferation rates of Mia Paca-2, Panc-1, and Patu 8988t pancreatic cancer cells with BCAT2 knockdown by shRNA. **n** = 4 biologically independent samples. **f.** Relative proliferation rates of Panc-1 and Patu 8988t pancreatic cancer cells with BCAT2 knockdown by CRISPR. **n** = 4 biologically independent samples. **g.** Mole percent enrichment (MPE) of BCAAs in hydrolyzed protein obtained from BCAT2 knockdown Mia Paca-2 cells cultured with ¹³C-BCKA. **n** = 4 biologically independent samples. **h.** FACS analysis of GFP-labeled Mia Paca-2 cells detected with Alexa 647-labeled antibodies to puromycin (puro-A647). **n** = 3 biologically independent samples. **i.** Representative images of SUnSET assay of Mia Paca-2 cells cultured in the indicated medium for 48h. Whole-cell lysates were subjected to western blotting with puromycin antibody. Experiments were repeated independently three times with similar results. **j.** CAF cocultures rescue the loss of growth in BCAT2-knockdown PDAC cells. **n** = 6 biologically independent samples. Data are presented as mean ± s.d. *P < 0.0001. Two-way ANOVA with Dunnett's multiple comparison test (b,e,f,j); multiple, two-tailed, unpaired, Student's *t*-test (d,g); One-way ANOVA with Tukey's post hoc comparison (h).

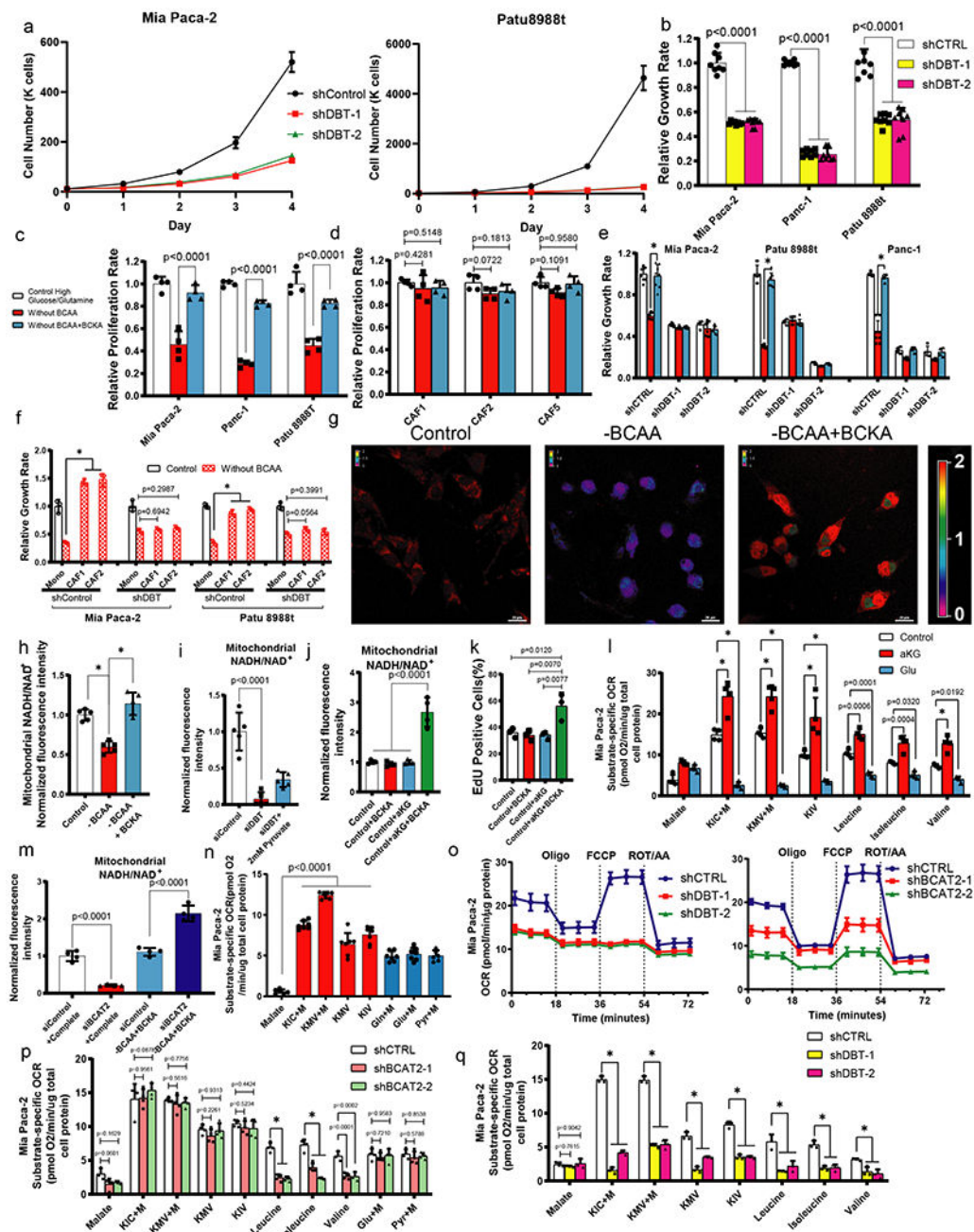


Fig. 3. BCKDH complex is essential for PDAC cell growth and cell biosynthesis.

a. Absolute cell numbers of PDAC cells expressing control shRNA or two independent shRNAs to DBT. $n = 3$ biologically independent samples. **b.** Colony-formation assay of DBT knockdown PDAC cell lines. $n = 3$ biologically independent samples. **c.** BCAA deprivation in the cancer monoculture can be rescued by BCKAs. $n = 4$ biologically independent samples. **d.** BCKA has no influence on CAF proliferation. $n = 4$ biologically independent samples. **e.** Relative proliferation rates of DBT knockdown cells in BCAA depleted media under BCKA replete conditions. $n = 8$ biologically independent samples. **f.** Relative proliferation rates of DBT knockdown cells co-cultured with CAFs. $n = 3$

biologically independent samples. **g-h.** NADH/NAD⁺ ratio measured using confocal fluorescence imaging of Mia Paca-2 cells in BCAA depleted media under BCKA replete conditions. n = 5 biologically independent samples. Experiments were repeated independently three times with similar results. **i.** NADH/NAD⁺ ratio measured using confocal fluorescence imaging of Mia Paca-2 cells transfected with siControl or siDBT. n = 5 biologically independent samples. **j.** NADH/NAD⁺ ratio measured using confocal fluorescence imaging of Mia Paca-2 cells in complete media with 4mM α KG added BCKAs n = 4 biologically independent samples. **k.** EdU uptake was measured in Mia Paca-2 cells in the presence of α KG and/or BCKAs after 1 day. n = 3 biologically independent samples. **l.** Substrate-specific oxygen consumption rate (OCR) in permeabilized pancreatic cancer cells measured using Seahorse Analyzer. n = 6 biologically independent samples. **m.** NADH/NAD⁺ ratio measured using confocal fluorescence imaging of Mia Paca-2 cells transfected with siControl or siBCAT2 in complete media or BCAA depleted media under BCKA replete conditions. n = 6 biologically independent samples. **n.** Substrate-specific OCR in permeabilized cells. n = 4 biologically independent samples. **o.** OCR measurements in DBT and BCAT2 knockdown cells. n = 6 biologically independent samples. **p.** Substrate-specific OCR measurements of BCAT2 knockdown cells. n = 4 biologically independent samples. **q.** Substrate-specific OCR measurement of DBT knockdown cells. n = 4 biologically independent samples. Data are presented as mean \pm s.d. *P < 0.0001. Multiple, two-tailed, unpaired, Student's *t*-test (b);two-way ANOVA with Dunnett's multiple comparison test (c,d,e,f,l,p,q); One-way ANOVA with Tukey's post hoc comparison (h,I,j,k,m,n).

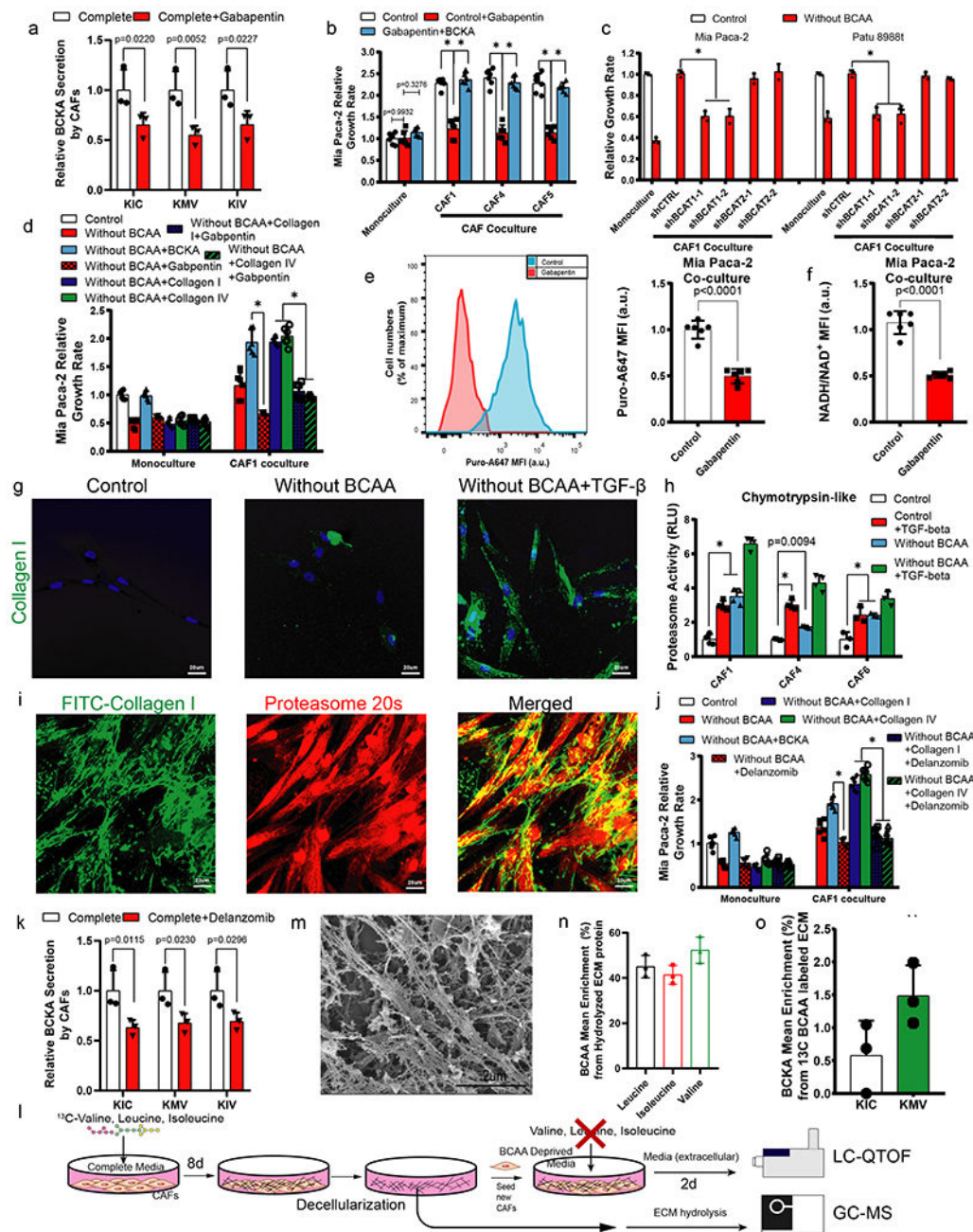


Fig. 4. BCAT1 regulates stromal cells' synthesis of ketoacids.

a. BCKA secretion by CAFs treated with 10mM Gabapentin. $n = 3$ biologically independent samples. **b.** Effect of 10mM Gabapentin on CAF-mediated rescue of MiaPaca-2 growth rate under BCAA deprived conditions. $n = 6$ biologically independent samples. **c.** Effect of BCAT1 and BCAT2 knockdown in CAFs using shRNA-BCAT1 and shRNA-BCAT2, respectively on CAF-mediated rescue of cell growth rate under BCAA deprivation. $n = 3$ biologically independent samples. **d.** Relative proliferation rates of Mia Paca-2 cells cocultured with CAFs and Collagen or 10mM Gabapentin under BCAA deprivation. $n = 6$ biologically independent samples. **e.** FACS analysis of GFP-labeled Mia Paca-2 cells

detected with puromycin antibodies in the co-culture system with 10mM Gabapentin. n = 6 biologically independent samples. **f.** Effect of 10mM Gabapentin on NADH/NAD⁺ ratio of cancer cells cocultured with CAFs. n = 6 biologically independent samples. **g.** Uptake of DQ-Collagen by CAFs assessed using confocal imaging after 24 h. Experiments were repeated independently three times with similar results. **h.** Proteasome activity in CAFs treated with TGF- β and under BCAA deprivation. n = 6 biologically independent samples. **i.** Colocalization of collagen and proteasome analyzed by immunofluorescence against 20S proteasome and FITC-collagen. Experiments were repeated independently three times with similar results. **j.** Relative proliferation rates of Mia Paca-2 pancreatic cancer cells cocultured with CAFs in combination with Collagen or Delanzomib under BCAA deprivation. n = 6 biologically independent samples. **k.** BCKA secretion by CAFs treated with Delanzomib. n = 3 biologically independent samples. **l.** Schematic of the protocol used to synthesize ECM labeled with ¹³C-BCAAs and secretion of ¹³C-BCKAs after culturing BCAA-deprived CAFs in ECM labeled with ¹³C-BCAAs. **m.** Scanning electron microscopy image of CAF-derived 3-D matrices. Experiments were repeated independently two times with similar results. **n.** Fractional enrichment of BCAAs after acid hydrolysis of decellularized ECM proteins produced by CAFs cultured with ¹³C-BCAAs. n = 3 biologically independent samples. **o.** Fractional enrichment of BCKAs secreted by CAFs after 48h of being cultured under BCAA deprivation on ECM labeled with ¹³C-BCAAs. n = 3 biologically independent samples. Data are presented as mean \pm s.d. *P < 0.0001. Multiple, two-tailed, unpaired, Student's *t*-test (a,k); two-tailed, unpaired, Student's *t*-test (e,f); two-way ANOVA with Dunnett's multiple comparison test (b,c,d,h,j).

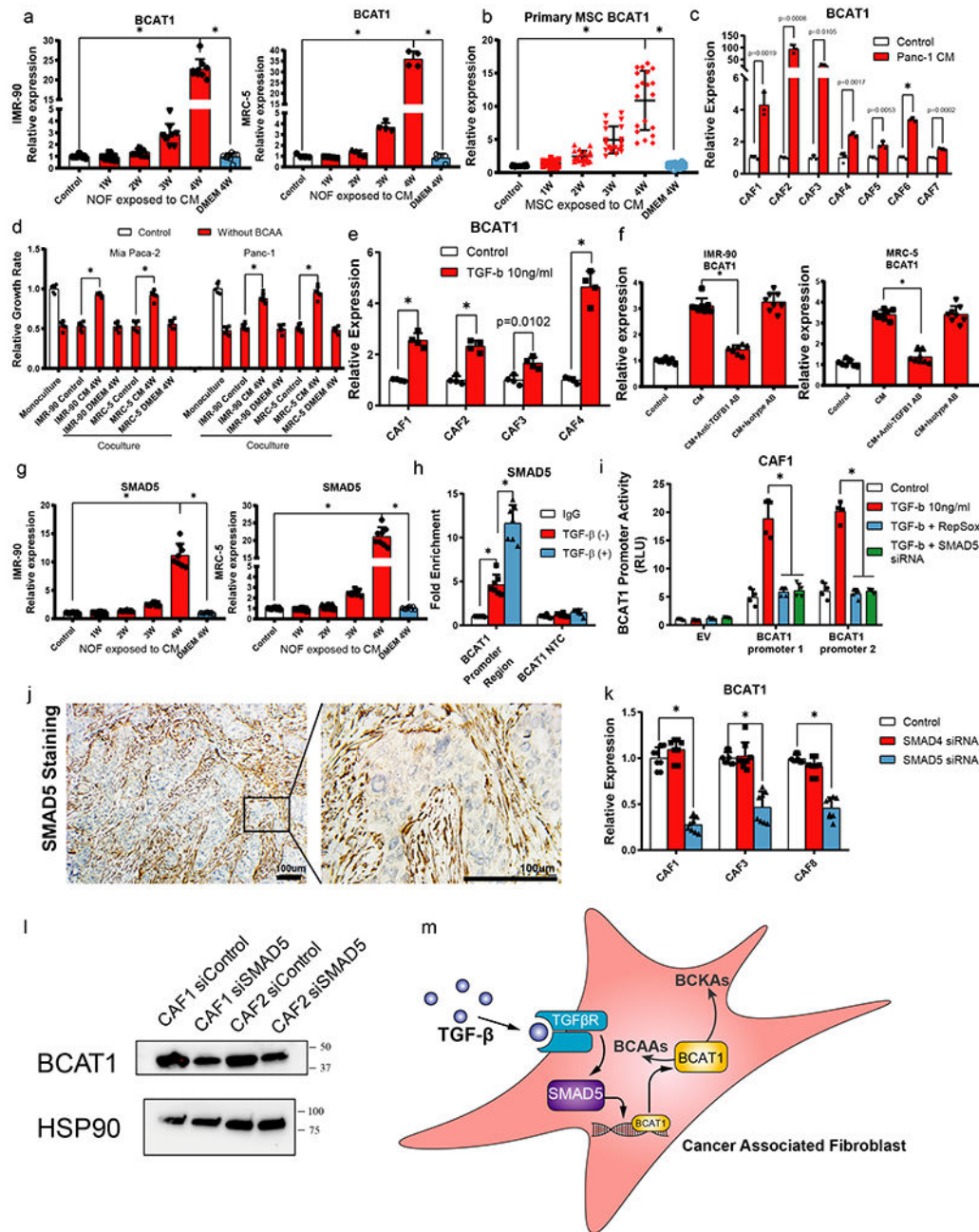


Fig. 5. Cancer cells regulate BCAT1 in stromal cells through TGF-β.

a. Effect of pancreatic cancer cell conditioned media (CM) on BCAT1 expression in NOFs over 4 weeks. *n* = 8 biologically independent samples. **b.** Effect of pancreatic cancer cell CM on BCAT1 expression in primary MSCs over 4 weeks. *n* = 6 biologically independent samples. **c.** Effect of pancreatic cancer cell CM on BCAT1 expression in various CAFs. *n* = 6 biologically independent samples. **d.** Growth rate of pancreatic cancer cells cultured with activated NOFs under BCAA deprivation. *n* = 6 biologically independent samples. **e.** BCAT1 mRNA expression measured in CAFs after 2 days of treatment with TGF-β. *n* = 6 biologically independent samples. **f.** BCAT1 expression in NOFs cultured with pancreatic

cancer cell-CM in the presence of neutralizing anti-TGF β 1 antibodies or isotype antibodies for 3 weeks. n = 8 biologically independent samples. **g.** Effect of pancreatic cancer cell CM on SMAD5 expression in NOFs over 4 weeks. n = 6 biologically independent samples. **h.** CHIP assays performed with control IgG and anti-SMAD5 antibodies in CAFs treated with PBS control or TGF- β . n = 4 biologically independent samples. **i.** Transient transfection assays in CAFs with the reporter plasmid containing BCAT1 promoter. n = 8 biologically independent samples. **j.** Representative IHC staining image comparing SMAD5 expression between stromal and tumor compartments. Experiments were repeated independently three times with similar results. **k.** mRNA expression of BCAT1 in CAFs treated with siRNAs targeting SMAD4 or SMAD5. n = 6 biologically independent samples. **l.** Immunoblots showing BCAT1 protein expression in CAFs treated with control siRNA and SMAD5 siRNA. Experiments were repeated independently three times with similar results. **m.** TGF- β secreted by cancer cells regulates BCAT1 expression in CAFs by activating SMAD5, which binds to the BCAT1 promoter. Data are presented as mean \pm s.d. *P < 0.0001. One-way ANOVA with Tukey's post hoc comparison (a,b,f,g,k); multiple, two-tailed, unpaired, Student's *t*-test (c,e); two-way ANOVA with Dunnett's multiple comparison test (d,h,i).

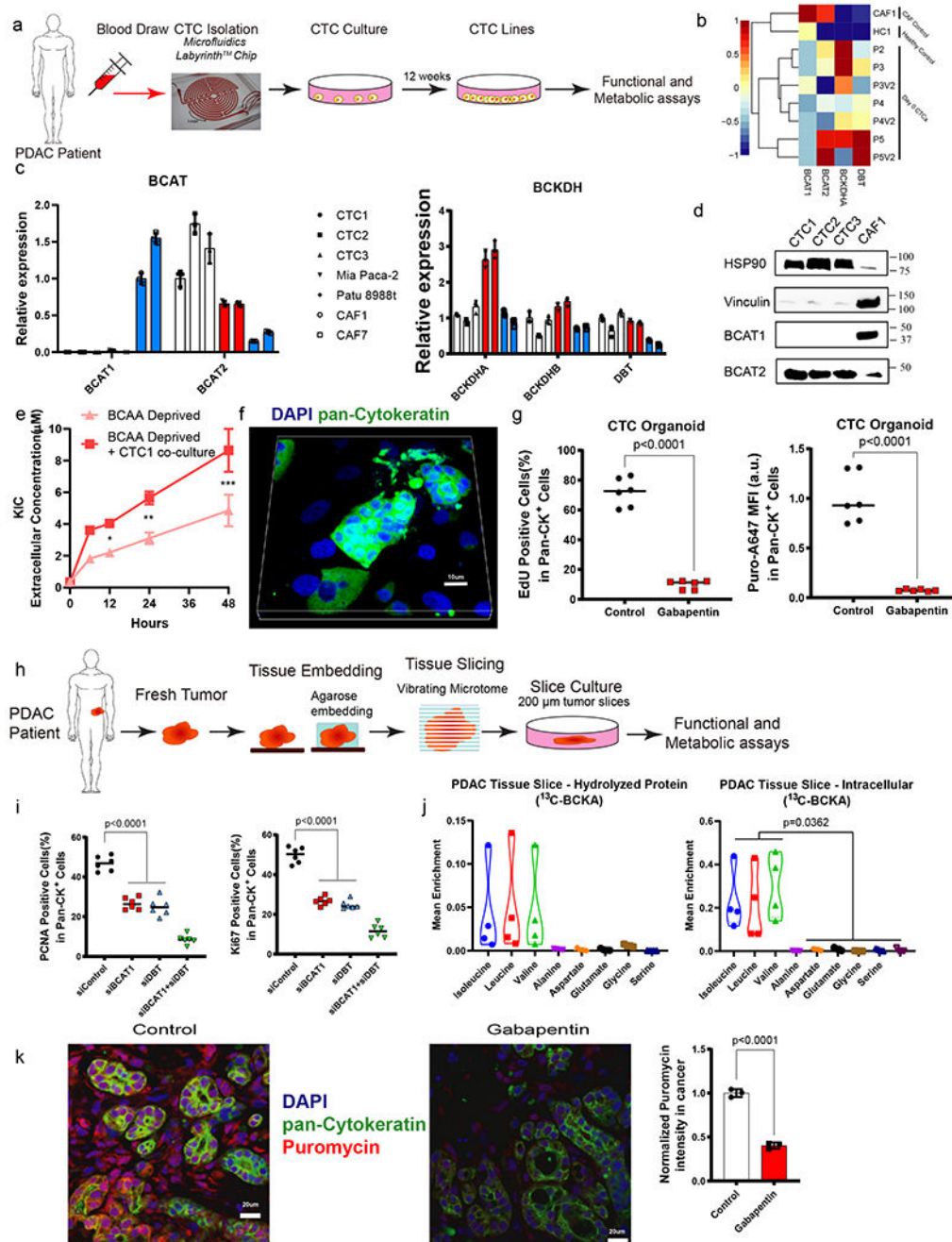


Fig. 6. Validation of stromal BCAT1 and PDAC DBT in patient-derived CTCs and tissue slices.
a. CTCs are isolated from the blood of PDAC patients using the microfluidics-based Labyrinth™ Chip. Isolated CTCs are purified to generate CTC cell-lines used for downstream analyses. **b.** Heatmap of gene expression of BCAT1, BCAT2, BCKDHA and DBT measured by qRT-PCR from Day 0 CTCs isolated from PDAC patients, CAF1 cells, and cells isolated from a healthy subject. $n = 7$ biologically independent samples. **c.** Relative BCAT1, BCAT2, BCKDHA, BCKDHB, and DBT mRNA expression determined by qRT-PCR in CAFs and patient-derived CTCs. $n = 4$ biologically independent samples. **d.** Immunoblots of BCAT1 and BCAT2 expression in CAFs and Patient-derived CTCs. HSP90

is used as loading control. Experiments were repeated independently three times with similar results. **e.** KIC concentration in spent media from CAFs in monoculture or cocultured with CTC line. $n = 3$ biologically independent samples. *, $p=0.0001$,**, $p=0.0008$,***, $p=0.0093$. **f.** Representative images from CTC derived organoid. Cytokeratin is shown in green and the nuclei stained with DAPI are shown in blue. Experiments were repeated independently three times with similar results. **g.** EdU staining and SUnSET assay on Pan Cytokeratin+ tumor cells in the CTC derived organoid cultured with CAFs treated with vehicle or 10mM Gabapentin. $n = 6$ biologically independent samples. **h.** Schematic of human PDAC tissue slice culture. Freshly biopsied tumor is embedded in agarose and sliced into 200 μm thick slices using a vibrating microtome. Slices are cultured for downstream metabolic and functional analyses. **i.** Percentage PCNA-positive and Ki67-positive in Pan Cytokeratin+ tumor cells identified using IF. $n = 6$ biologically independent samples. **j.** Fractional enrichment of BCAAs of human PDAC tissue slices cultured with ^{13}C -BCKAs. $n = 5$ individual tissue samples from distinct patients. Violin plot represents entire range of values, lines at median, 10-90 percentiles. **k.** Representative images from SUnSET IF analysis of PDAC tissue treated with vehicle or 10mM Gabapentin. $n = 3$ biologically independent samples. Data are presented as mean \pm s.d. except **j.** * $P < 0.0001$ except **e.** Multiple, two-tailed, unpaired, Student's t -test (**e**); two-tailed, unpaired, Student's t -test (**g,k**); one-way ANOVA with Tukey's post hoc comparison (**I,j**).